Chair of Materials Science and Testing of Polymers

Master's Thesis

Evaluation of the influence of material, manufacturing and testing parameters on the leakage of PTFE and PEEK based sealing materials in reciprocating compressors

Micha Humpel, BSc

October 2019

AFFIDAVIT

I declare on oath that I wrote this thesis independently, did not use other than the specified sources and aids, and did not otherwise use any unauthorized aids.

I declare that I have read, understood, and complied with the guidelines of the senate of the Montanuniversität Leoben for "Good Scientific Practice".

Furthermore, I declare that the electronic and printed version of the submitted thesis are identical, both, formally and with regard to content.

Date 11.11.2019

Signature Author
Micha, Humpel

Abstract

The pressure packing seals the compression chamber of a reciprocating compressor from the environment and is a performance determining component. The pressure packing consists of several containers, also called cups, in which a sealing element is placed. Such a sealing element typically consists of one or more packing rings. The packing rings are designed such, that they can compensate wear geometrically. The sealing element (ring group) is activated by the differential pressure that it seals. The pressure differential over a ring group presses the ring segments against each other and the rings against the piston rod and the cup face. The contact pressure between these surfaces is determined by the pressure differential and the ring geometry. The contact pressure and the gas pressure are in the same order of magnitude. Leakage through a packing ring group can occur in multiple places:

- In the dynamic sealing surface between the reciprocating rod and the seal.
- In the static sealing surface between a ring and another ring or a ring and the cup.
- Due to manufacturing imperfections on the edges between ring segments or between packing rings.

The aim of this thesis is to study the impact of various testing, material and manufacturing parameters on the face-to-face sealing elements. The focus lies on the applied gas pressure and the contact pressure and the roughness and flatness.

A test rig was designed to test the impact of those parameters on the leakage. The test rig allows a defined application of the contact pressure, which is independent of the application of the gas pressure. Possible leakage is recorded end-of-line. In order to test the influence of flatness and roughness, specimens were produced with different machining methods and parameters. Based on material combinations, which are typically used in a sealing element, a design of experiments was introduced to test different materials and different sealing surfaces.

Influencing parameters other than the intended ones were studied and minimized, where possible, before the tests were performed. The developed measurement routine was used for all tested material combinations.

The theoretically expected dependencies of the leakage on the contact pressure and the gas pressure were confirmed. Leakage decreases logarithmically with increasing contact pressures. For gas pressures smaller than the contact pressure a linear increase of leakage with increasing gas pressure is detected. As soon as the gas pressure equals the contact pressure its influence on the contact situation cannot be neglected any more and leakage increases more rapidly.
For soft materials the roughness plays an important role. Finer surfaces result in less leakage. The flatness is more important for rigid materials as the rings are not as easily deformed. This is especially relevant for low contact pressures.

Kurzfassung

Die Druckpackung eines Kolbenkompressors hat die Aufgabe den Verdichtungsraum zur Umgebung hin abzudichten. Sie ist eine Peformance-bestimmende Komponente. Die Druckpackung besteht aus mehreren Abschnitten, die als "Container" oder als "Cup" bezeichnet werden. In jedem Abschnitt befindet sich ein Dichtelement. Diese Dichtelemente setzen sich aus einem oder mehreren Packungsringen zusammen. Das Dichtelement, das auch als Ringgruppe bezeichnet werden kann, wird durch den abzudichtenden Differentialdruck aktiviert. Durch die Druckdifferenz werden die einzelnen Ringsegmente aufeinander, auf die Kolbenstange und gegen die Oberfläche des Cups gedrückt. Der Kontaktdruck zwischen den Oberflächen ergibt sich aus der Druckdifferenz und der Ringgeometrie und liegt in der Größenordnung des Gasdrucks. Leckage durch ein Dichtelement kann an mehreren Stellen auftreten:

- In der dynamischen Dichtfläche zwischen der sich bewegenden Kolbenstange und dem Dichtelement.
- In der statischen Dichtfläche zwischen einem Ring und einem weiteren Ring oder einem Ring und der Cup-Oberfläche.
- Aufgrund von herstellbedingten Imperfektionen an den Kanten zwischen den einzelenen Ringsegmenten und zwischen einzelnen Packungsringen.

Die vorliegende Arbeit untersucht die Leckagepfade zwischen statischen Dichtflächen und den Einfluss von Test-, Material- und Bearbeitungsparametern auf die Leckage. Der Fokus liegt dabei auf dem Kontaktdruck, dem anliegenden Gasdruck und der Rauigkeit und Flachheit der Dichtringe.

Um diese Einflüsse zu testen wurde ein Teststand gefertigt. Mithilfe einer Zugprüfmaschine kann ein definierter Kontaktdruck unabhängig vom anliegenden Gasdruck aufgebracht werden. Etwaige Leckage wird am Ende des Prüfaufbaus gemessen. Die Dichtringe wurden mit verschiedenen Berarbeitungsmethoden und -parametern hergestellt, um den Einfluss der Rauheit und der Flachheit auf die Leckage zu untersuchen. Verschiedene Materialpaarungen, die typischerweise auch in Dichtpackungen verwendet werden, wurden im Zuge eines Versuchsplans vermessen.

Bevor die Testreihe durchgeführt wurde, wurden störende Einflussfaktoren im Versuchsaufbau detektiert und minimiert. Das entwickelte Messschema wurde für alle Materialkombinationen verwendet.

Die Versuche bestätigten die theoretischen Zusammenhänge. Die Leckage nimmt logarithmisch mit zunehmendem Kontaktdruck ab. Für den Fall, dass der anliegende Gasdruck geringer als der Kontaktdruck ist, kommt es zu einem linearen Anstieg der Leckage mit zunehmendem Gasdruck. Sobald der Gasdruck im Bereich des Kontaktdrucks liegt, kann dessen Einfluss auf den Kontakt zwischen den Dichtringen nicht mehr vernachlässigt werden. Dies resultiert in einem schnelleren Anstieg der Leckage.

Für leicht deformierbare Materialen spielt die Flachheit nur eine untergeordnete Rolle und die Rauigkeit ist der treibende Faktor. Für steifere Materialien spielt die Flachheit eine größere Rolle. Vor allem bei geringem Kontaktdruck können dadurch Spalte zwischen den Dichtelementen entstehen, was zu sehr hohen Leckagen führt.

Acknowledgement

First and foremost I thank HOERBIGER Wien GmbH for the opportunity to conduct my master thesis in this interesting application-oriented field of research. Special thanks goes to Dr.mont. Dipl.-Ing. Andreas Kaufmann and Dr.mont. Dipl.-Ing. Marian Janko for their supervision and help throughout the process. Their insights and inputs helped moving forward in the right direction. I thank the whole Hoerbiger R&D team for their support and the collective coffee breaks. Furthermore I thank the R&D workshop; without their help, conducting the research would literally have been impossible.

Secondly I thank Univ.-Prof. Dr.mont. Dipl.-Ing. Gerald Pinter, the Head of Chair of Material Science and Testing of Polymers, for his efforts and for giving me the opportunity to write this thesis in cooperation with HOERBIGER Wien GmbH.

Probably the biggest thanks goes to all my friends and study colleagues for always being there for me, the endless study sessions and the exciting evenings. Thank you for making the last couple of years so special.

Last but not least, I thank my whole family for their support during my studies and during the course of the work for this thesis.

Contents

1 Introduction

The industry always calls for more efficient and reliable compressors. The sealing elements are necessary for an efficient operation and have to function in different operating conditions and environments. A failure of packing rings results in expensive downtime of the whole compressor or even the whole process line. Reciprocating compressors are used in multiple fields of application, like in the oil and gas industry, PET blow molding and in the chemical industry. Depending on the compressed gas, leakage has to be minimized, not only to increase the efficiency of the compressor, but also to prohibit an escape of the compressed gas into the environment. This is achieved by the main pressure packing, which consists of several containers, also called cups. Each packing container contributes differently to the whole pressure reduction. The exact contribution of each container to the overall pressure reduction is generally unknown.

The sealing mechanism is often referred to as "self-energizing". The rings are pressed onto the piston rod, other rings and the cup face by the existing pressure differential. The contact pressure between the components is determined by the pressure differential and the geometry of the segmented rings. The leakage through the sealing elements can be classified into different sections:

- Leakage through the dynamic sealing surface between the reciprocating rod and the rings.
- Leakage through the static sealing surface between the faces of a ring and another ring or the cup.
- Leakage in the joints of segmented rings.

Relative motion between the rings and the piston rod occurs, which results in a dynamic sealing surface. The faces of the rings and the ring segments do not significantly move relative to each other resulting in a static sealing surface. The leakage through face-to-face contacts occurs due to the surface roughness. Leakage through the joints occurs due to manufacturing imperfection on the edges. Although the contact situation is simpler for static sealing surfaces, the influence of various parameters on the leakage is not well researched. The objective of this thesis is to gain knowledge of the influence of the pressures and the surface quality on the leakage. Additionally, in compressors the amount of leakage through each possible leak path is not known. With these experiments, the order of magnitude of leakage through face seal rings, where no relative motion occurs, is obtained. Compared to the typical total leakage through the main pressure packing, a statement about which leakage paths are more critical can be made. Therefore a test sequence and a design of experiments were introduced to cover all these aspects.

2 State of the Art

This chapter focuses on the sealing mechanisms of the pressure packing in reciprocating compressors. It shows the possible leakage paths and the ones tackled in this thesis. Furthermore it gives an overview of the state of the art designs and materials for packing rings. Often the terms sealing rings and packing rings are used interchangeable. In this thesis a distinction between the terms is made. By the term packing rings cut or uncut rings as used in the actual application are referenced. Sealing rings are uncut rings as they are used in this thesis and described in Chapter 4.2.

Compressors are used to move gases from one place to another. Reciprocating compressors are one of the most common compressor types. The gas is compressed by a positive displacement using a piston, cylinder and an arrangement of valves. [1, 2]

Figure 1 shows the most important components of reciprocating compressors. In order to perform the compression task various sealing elements are necessary. Valves and rings are both dynamic sealing elements, but the meaning of the term dynamic is a different one. Valves move dynamically between a seat and a guard and only seal when the plate contacts the seat. For packing rings there is a relative motion between the rings and the piston rod and for piston rings the relative motion occurs between the rings and the liner. Packing and piston rings have the same working principle, face a similar situation during the compression and seal the compression chamber. Only the pressure packing will be discussed in further detail. [3]

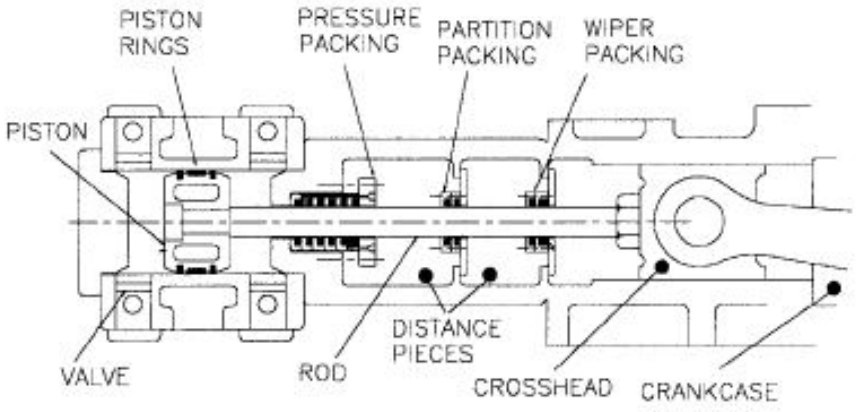

Figure 1: Main components of a reciprocating compressor [4].

2.1 Main Pressure Packing

In order to fulfill its function, sealing the compression chamber to the environment along the reciprocating piston rod, the main pressure packing consists of a series of seal rings. Figure 2 shows the cut through a typical pressure packing, which consists of several cups, each holding a sealing element that may consist of several rings of different geometry. The packing rings are pressed against the rod and the face of the next cup by the existing differential pressure. Leakage cannot be completely prevented, but should be reduced as much as possible. [3, 4]

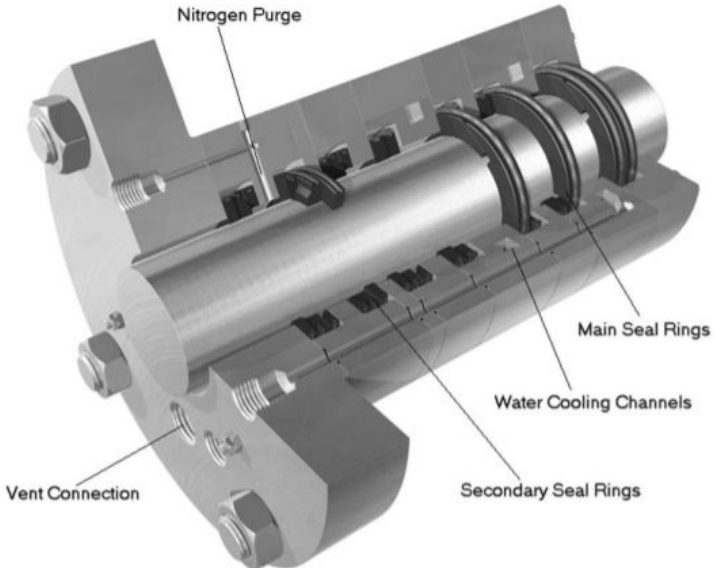

Figure 2: Cut through pressure packing [5].

Which part each individual cup contributes to the whole sealing is controversial. Hanlon [4] states that for a new set of rings the pressure drop is highest for rings nearest to the piston. As in this theory most pressure is acting on the rings nearest to the piston, those rings wear faster. Rings, which are located further away from the piston, are exposed to smaller pressure differentials and do not wear as fast. Once the packing rings, which are nearer to the piston wear, their share to the complete pressure drop will decrease and the pressure break reduction will shift to the following cups. More recent studies [6, 7] come to the conclusion that the contribution of each cup to the total pressure drop is far more complicated. In addition to wear, the differential pressure and the time that it exists are influencing the pressure drop pattern.

2.2 Designs of Pressure Packing Rings

Packing rings are the most important part of the pressure packing, as they ensure sufficient sealing. In order to compensate wear, seal rings have to be cut into sep-

arate pieces. Various designs of such cut rings can be seen in Figure 3. Often ring groups consisting of a radial (a) and a tangential (b) cut ring are used. Both ring types consist of three identical segments. A clearance gap between the ring segments is necessary to compensate wear, so that the segments close when wear occurs. This clearance gap provides a direct leakage path and a combination of rings is necessary to ensure the sealing function. One of the simplest combinations is a radial cut ring (R), which faces the high pressure side, and a tangential cut ring (T), which faces the low pressure side. In order to function, the two rings are aligned, such that no direct leakage path through the clearance gaps exist. The mating surfaces of the two rings must contact each other and the tangential ring must be in contact with the sealing face of the cup (C). [1,4] Figure 4a shows such a combination schematically.

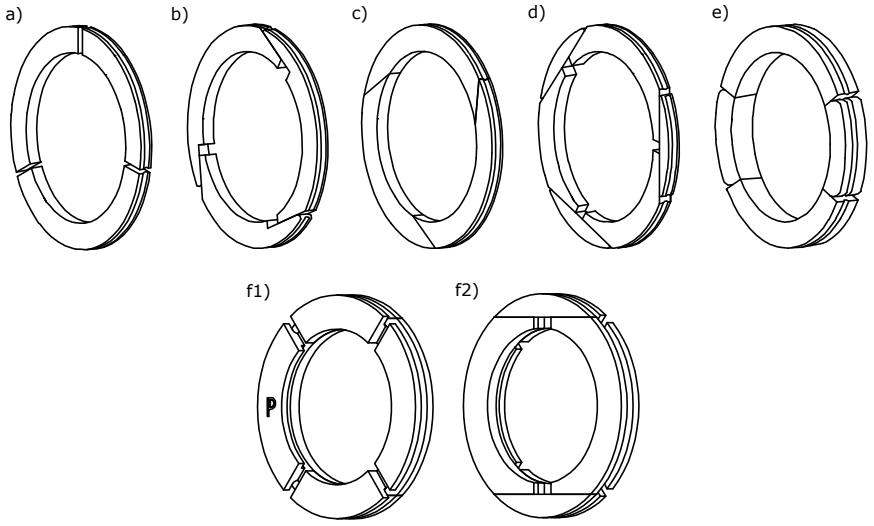

Figure 3: Typical designs of pressure packing rings: a) 3 piece radial cut ring, b) 3 piece tangential cut ring with wear stop, c) 3 piece tangential to rod cut ring without wear stop, d) 6 piece tangential cut ring, e) 4 piece ring design f) balanced cap design (BCD) ring (f1 shows the pressure side, f2 the sealing side) [3].

More designs of sealing rings can be seen in Figure 3. The more recently developed balanced cap design (BCD) stands out, as this single ring provides no direct leakage path. Its more compact design allows shorter packings. [3]

Higher temperatures and pressures increase the probability that the polymeric sealing ring creeps into the radial clearance gap between the cup and the piston rod. This can have negative effects on the operating system, like higher temperatures due to higher frictional forces and shorter life time of the rings. To reduce this effect backup rings are used. They are usually made out of metals and are uncut or three piece radially cut rings, see Figure 5. The clearance to the piston rod is usually a few tenth of a millimetre [3]. A typical packing ring group with a backup ring (B) is shown in Figure 4b.

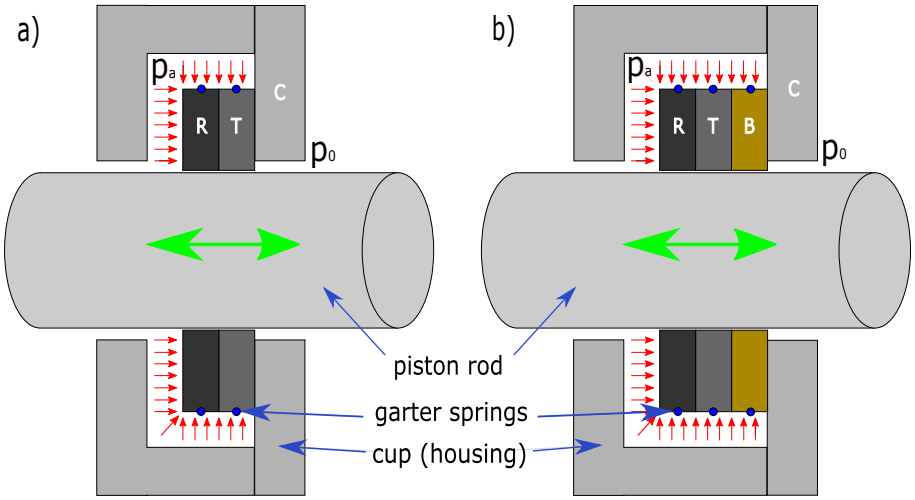

Figure 4: Typical packing ring groups consisting of a radial and a tangential cut ring without (a) and with (b) a backup ring. R ... radial cut ring, T ... tangential cut ring, B ... backup ring, C ... cup (sealing face), p_a ... gas pressure (before packing ring group), p_0 ... gas pressure (after packing ring group)

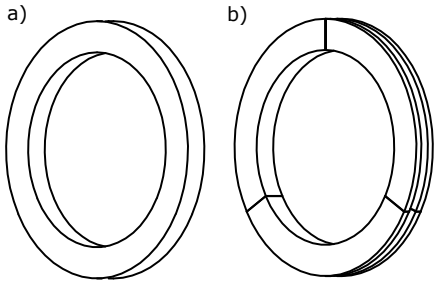

Figure 5: Typical designs of backup rings: a) uncut backup ring, b) three piece radial cut backup ring [3].

2.3 Materials Used in Pressure Packings

The above discussed characteristics of pressure packings are true for both lubricated and non-lubricated compressors. The selection of packing ring materials is mainly influenced by lubrication, gas pressure and gas type. This section focuses on materials used in non-lubricated compressors. While backup rings are often made of metals, the actual sealing rings are mostly made of filled polymers and polymer blends. They can be classified as fluoropolymers, polymer blends and high temperature polymers. [8]

The most often used fluoropolymer polytetrafluorethylene (PTFE) offers good self-lubrication properties, but inferior mechanical properties. Advantages of PTFE are [8]:

- its high ductility,
- its low coefficient of friction,
- its good chemical resistance,
- that no stick-slip-effect occurs,
- that it shows almost no moisture absorption and
- that it is non-toxic.

As PTFE has a high creep tendency and shows a rapid decrease in strength with increasing temperatures, it is not used in its pure form. To minimize those effects various fillers can be added. Frequently used fillers are amorphous carbon, graphite, glass and carbon fibres and metals like copper and bronze. Detailed compositions are well protected secrets of the various manufacturers. [8]

For higher temperatures and pressure differentials high temperature polymers are often used. Commonly used materials are polyether ether ketone (PEEK), polyphenylene sulphide (PPS), polyimide (PI) and polyamide imide (PAI). Their good mechanical properties even at high temperatures come with inferior lubrication properties. Pure they cannot be used in non-lubricated compressors. Therefore they have to be modified by adding solid lubricants like carbon, graphite, PTFE or molybdenum disulphide. [8]

For applications, where the base polymer does not achieve the necessary properties, polymer blends can be used. Additionally to the already mentioned non-polymeric fillers PTFE can be blended with a high temperature polymer. The properties of the blend are superior to the properties of the base materials. [8]

As backup rings should prevent extrusion of the polymer sealing ring into the clearance gap between the cup and the piston rod, materials with less creep tendency are used. Frequently bronze is chosen, but other metals or high performance polymers can be used as well. [3]

2.4 Pressure Situation in a Packing Case

Kaufmann [3] studied the pressure situation in a packing case. For simplification, a cup with with only one ring is considered. Step by step, Figure 6 shows the composition of the pressures in the sealing surfaces and the wear relevant contact pressure distribution. p_{cyl} denotes the pressure acting on the ring from side of the cylinder, p_{crk} the pressure on the crank side. The gas pressure differential p_{cyl} - p_{crk}, which acts on the ring can be seen in Figure 6a. Surfaces, which are nominally flat on a micro- and macroscopic scale, result in a theoretical contact pressure between the sealing surfaces $p_{\mathrm{c,flat}}$ (Figure 6b). As all machined surfaces show some degree of surface roughness, the gas can creep into the interface, resulting in a pressure distribution p_{g} that counteracts the theoretical contact pressure, which is shown in

Figure 6c. Therefore the theoretical contact pressure $p_{\mathrm{c,flat}}$ is reduced by the interfacial gas pressure p_{g}. This results in a remaining theoretical contact pressure $p_{\mathrm{c,rough}}$ for rough surfaces. In Figure 6d the complete pressure situation can be seen and the resulting apparent contact pressure is marked green.

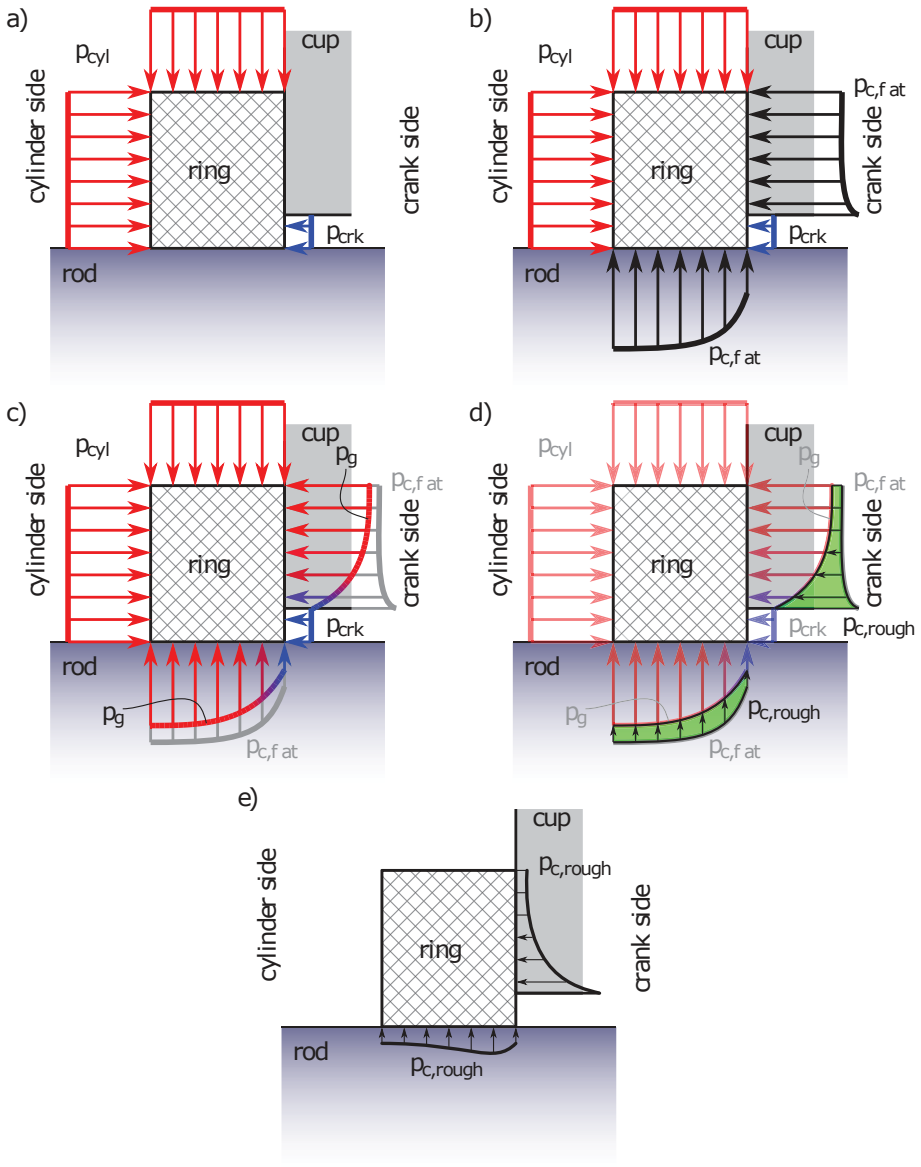

Figure 6: Typical gas and contact pressure situation in a container. a) Prevalent gas pressure differential p_{cyl} - p_{crk}, b) resulting contact pressure between the ring and cup and ring and rod for micro- and macroscopic perfectly flat surfaces $_{\mathrm{c,flat}}$, c) gas pressure profile at the interfaces due to surface roughness p_{g}, d) full pressure situation with the resulting contact pressure $p_{\mathrm{c,rough}}$ and e) isolated contact pressure between ring and cup and ring and rod $p_{\mathrm{c,rough}}$ [3].

The pressure distribution that results from gas creeping in between the asperities of the surfaces can be mathematically described by a Hele-Shaw flow. In this model the gap between the two rough surfaces can be replaced by a gap with an equivalent constant thickness. When the pressure drop across the gap cannot be neglected, gas compressibility effects play a dominant role. [3] The pressure distribution in this case can mathematically be described by

$$\nabla^2 p_{\mathrm{g}}^2 = 0, \tag{1}$$

where ∇^2 is the Laplace operator and p_{g} the gas pressure profile at the sealing interface.

2.5 Leakage in the Pressure Packing

There are multiple possible leakage paths through a packing ring group. Due to the "self-energizing" working principle, the pressure differential, which needs to be sealed, and the contact pressures between the rings, the cup and the rod cannot be set independently. The contact pressures are dependent on the existing differential pressure, the ring geometry and friction. Increasing the contact pressure by changing the geometry is possible, but also influences wear. Therefore contact pressures cannot be increased arbitrarily and contact pressures and gas pressures will be in the same order of magnitude, where leakage of some degree is inevitable.

Possible leakage paths in an activated packing ring group are between the faces of two sealing rings, a ring and cup face, in between the ring segments of a single ring and along the piston rod in the dynamic sealing surface. [4]

As soon as relative motion is introduced, the mechanisms of contact change. The penetration of the asperities of the harder surface in addition to a sliding motion results in plowing of the softer material. In between the two surfaces an interfacial layer is formed that highly influences the contact and sliding mechanism and therefore the formation of leakage paths. [9] The focus in this thesis lies on leakage paths, where no relative motion occurs between the sealing surfaces. Further details on the mechanism of sliding friction can be found in Bhushan [9].

It is believed that most leakage through non-dynamic sealing surfaces occurs in the joints within a ring due to misfits. Figure 7 shows possible leakage paths formed by machining imperfections. As there is no such thing as perfect machining, leakage will always occur. Leakage due to insufficient surface finishes of the ring faces does also occur, but it is believed that leakage paths are smaller. [4]

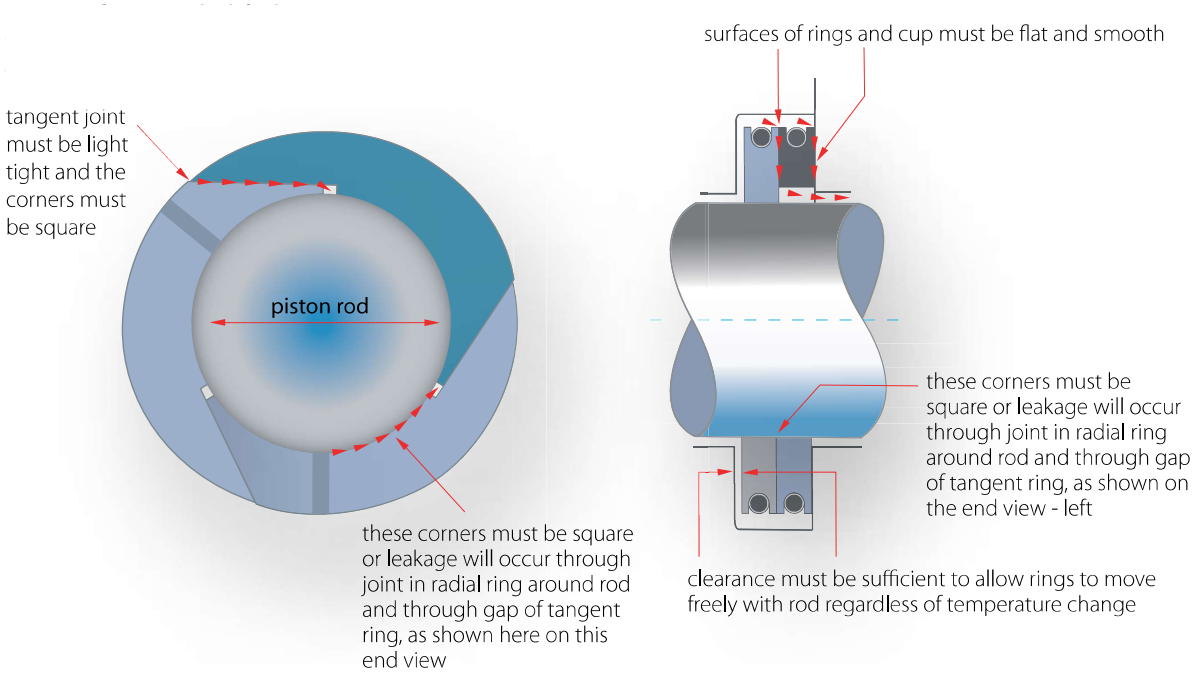

Figure 7: Possible leakage paths formed by machining imperfections [7].

3 Theoretical Background

This chapter introduces surface parameters that can be used to describe surfaces and that are used in this thesis. Furthermore, the contact mechanic principles, on which the sealing problem is base ond, are introduced. Factors influencing the leakage of static sealing surfaces and methods to describe leakage as a function of material and surface parameters are then discussed. There is a variety of parameters that influence the leakage in static seals. They can be classified as surface topography, material, testing (in the application: process) and other parameters. [10]

3.1 Characterization of Surfaces

This section gives an overview of parameters that can be used to describe nominally flat surfaces. Out of the numerous parameters that are available, the ones that are used in contact mechanics and leakage modelling are selected and discussed.

Machining processes are not able to produce perfectly flat surfaces. Produced surfaces consist of a complex structure. The resulting surface texture is defined as

> *"the repetitive or random deviation from the nominal surface that forms the threedimensional topography of the surface."* [11]

Surface texture can be classified in [11]:

- roughness,
- waviness,
- lay and
- flaws.

All of the above influence the leakage in seals. These parameters can be calculated from a line measurement (1D-profile) or an areal measurement (2D-surface) with tactile or optical methods. Two dimensional measurements give additional information about the surface. For example, lay, the anisotropy of roughness, which is caused by some manufacturing methods, can be detected. [12] 1D-roughness parameters are used in the experimental part, because of the availability and ease of use of tactile profilometers.

Qu [13] investigated, which roughness parameters can distinguish between leaking and not leaking parts in a radial lip seal application. As the operating principle is similar to the test method used in this thesis, the parameters should be applicable. The research found that the maximum depth of valleys R_{v}, the skewness R_{sk} and the kurtosis R_{ku} are capable of predicting if the seal will leak. [13] Additionally, the arithmetic average height R_{a}, the power spectral density and the root mean square

slope of the surface profile R_{dq} are further discussed.

The traditionally most used parameter for seals is the **arithmetic average height** $R_{\mathbf{a}}$. [13] It is defined as

$$R_{\mathrm{a}} = \frac{1}{l} \int_0^l y(x)\ dx. \tag{2}$$

where l is the sample length and $y(x)$ is the measured profile. As long as the mean lines of measured profiles are the same, also R_{a} will be the same. Figure 8 shows that even for totally different surface profiles the R_{a} value can be the same. Profile 2 may result in rather low leakage rates, because its few sharp peaks can be deformed. Profile 1 may result in non tolerable leakage, as the valleys provide a leakage path. Therefore controlling only the R_{a} value may not be sufficient.

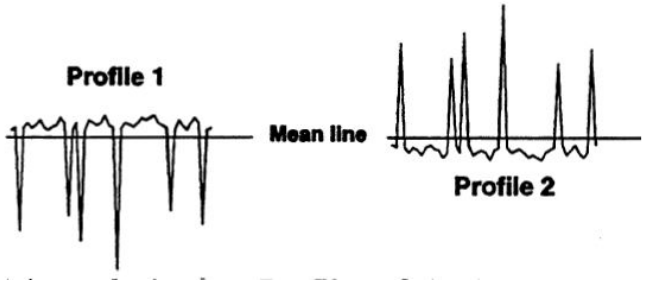

Figure 8: Different surface profiles with the same R_{a} value [13].

The **maximum depth of valleys** $R_{\mathbf{v}}$ is the distance from the maximum depth in the assessed length to the mean line. [12]

For the definition of the skewness and kurtosis other roughness parameters are necessary. R_{q} is the **root-mean-square roughness**. It describes the distribution of surface heights and can be seen as the standard deviation of it. Therefore it is an important parameter for statistical description of a profile. [12] It is defined as

$$R_{\mathrm{q}} = \sqrt{\frac{1}{l} \int_0^l \{y_(x)\}^2\ dx}. \tag{3}$$

Kurtosis and skewness are often referred to as statistical parameters. To measure the statistical distribution of the profile, the profile probability density function $p(y)$ is introduced, which is the derivative of the cumulative probability distribution function $P(t)$. In general this function gives the probability of the event $y(x) \leq t$. For a surface profile, $P(t)$ gives the probability, that the distance from the mean line to a random point on the profile $y(x)$ is smaller than a defined distance t from the mean line. [9] It can be written as

$$P(t) = Prob(y \leq t). \tag{4}$$

Therefore the probability density function is

$$p(y) = \frac{dP(t)}{dy}. \tag{5}$$

In the case of statistical surface characterization, the probability density function turns into an amplitude density function, which can be seen as the distribution histogram of the surface heights. This distribution is obtained by plotting the profile heights against their density. Frequently a standardized Gaussian distribution is used for the probability density function. [12] Further details on the statistical probability distribution and density function can be found in Bhushan [9].

The third central moment of the amplitude probability function is called **skewness** $R_{\mathbf{sk}}$. It describes the symmetry of the profile about the mean line. It is dependent on high profile peaks or low profile valleys. Examples of profile curves with their according distribution curves can be seen in Figure 9. If the bulk of material is above the mean line the skewness is negative and vice versa. [11, 12] The mathematical definition of the skewness is

$$R_{\mathrm{sk}} = \frac{1}{R_{\mathrm{q}}^3} \int_{-\infty}^{\infty} y^3 p(y)\, dy. \tag{6}$$

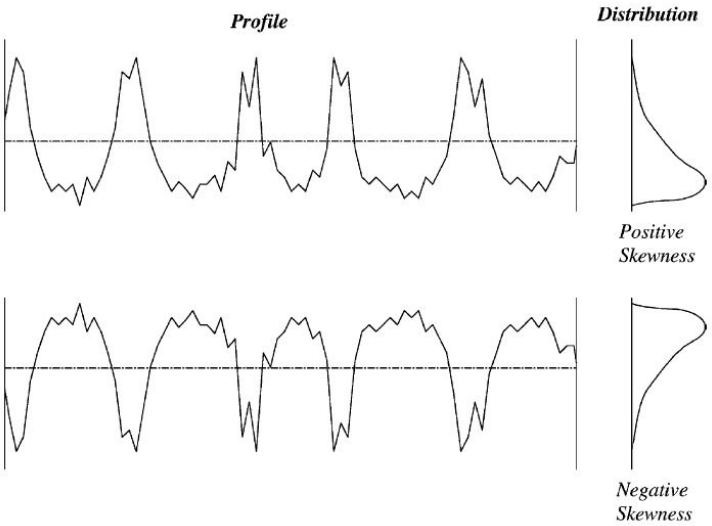

Figure 9: Different profiles with their according distribution curves to define skewness [12].

Similar to the skewness, the **kurtosis** $R_{\mathbf{ku}}$ is the fourth central moment of the amplitude probability function. It is used to define the sharpness of the profile. Examples of profiles with their according distribution curve are shown in Figure 10

to illustrate the influence of the sharpness of the profile. [11, 12] The kurtosis can be calculated as shown in Equation 7.

$$R_{\mathrm{ku}} = \frac{1}{R_{\mathrm{q}}^4} \int_{-\infty}^{\infty} y^4 p(y)\, dy \tag{7}$$

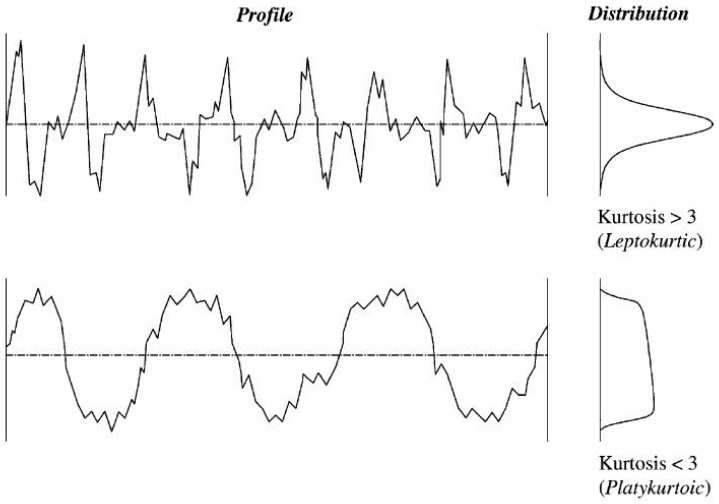

Figure 10: Different profiles with their according distribution curves to illustrate the influence of the sharpness [12].

Another method to describe a surface roughness profile is separating it into contributions from different spatial frequencies, also called wavevectors q. This descriptive method is called power spectral density, which mathematically can be seen as the Fourier transform of the autocorrelation function. [14] The mathematical derivation of the autocorrelation function and the power spectral density can be found in Bhushan [9].

The principle that describes how the **power spectral density** C_{q} is obtained, is shown in Figure 11 for a superposition of two sine waves, (a) and (d), a frozen capillary wave and panel, (b) and (e) and a self affine, randomly rough surface, (c) and (f). The root mean square height S_{q} ($\widehat{=}R_{\mathrm{q}}$) is the same for each surface. The profile is split into contributions from different wavevectors and for each wave length the power spectral density is obtained and plotted. Analysis of the surface roughness on different length scales are necessary to obtain a full plot. [14]

The **root mean square slope of the surface profile** R_{dq} is defined as the root mean square of slopes of the assessed profile [12]. It is used in the elastic contact mechanics, which is introduced in Chapter 3.2. The mathematical definition can be found in Equation 8, where $\Theta(x)$ is the slope of the profile at the position x.

$$R_{\mathrm{dq}} = \sqrt{\frac{1}{l}\int_0^l (\Theta(x))^2 \, dx} \tag{8}$$

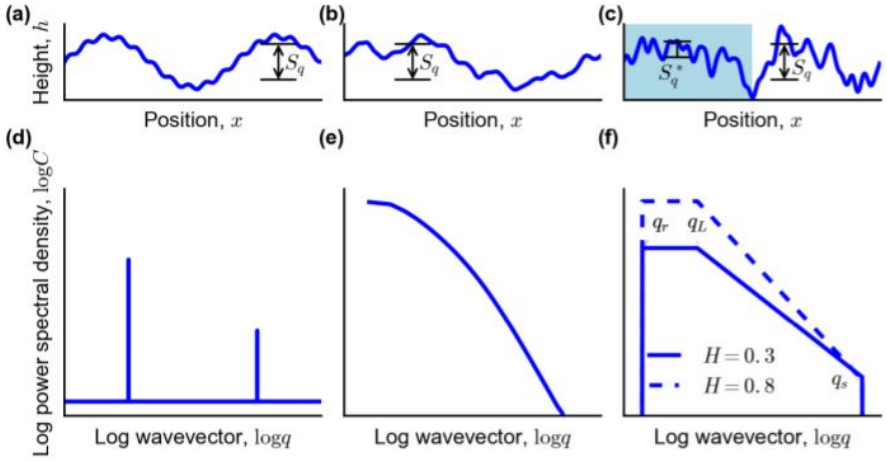

Figure 11: Examples of the power spectral density for different profiles: (a) and (d) superposition of two sine waves, (b) and (e) a frozen capillary wave and panel, (c) and (f) self affine, randomly rough surface [14].

On a larger length scale, deviations from the true surface are considered geometrical errors. For flat surfaces the used parameter is the **flatness** [15]. Figure 12 illustrates how it is obtained. The flatness deviation is defined as

"the minimum distance separating two parallel planes between which the surface can be contained." [15]

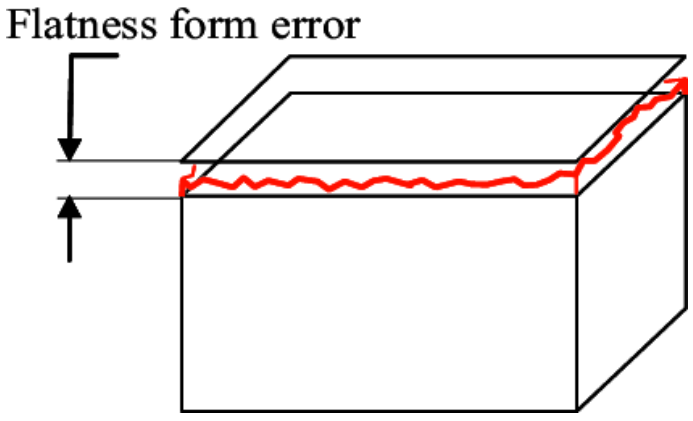

Figure 12: Visualization of the definition of flatness. The true surface is marked red [16].

3.2 Elastic and Plastic Contact Mechanics

When two bodies are pressed together, elastic and plastic changes in shape will occur. This process can be viewed at macroscopic and microscopic scales. To understand the influence on the sealing, both aspects of contact mechanics have to be taken into account. [9, 11]

On a macroscopic scale the contact of seals can be seen as two macroscopic flat surfaces pressed together. To understand this principle a flat planar punch, which is shown in Figure 13, is considered. A surface of a rigid body with a width in x-direction of $2b$ and an infinite length in y-direction, which is pressed on an elastic half-space with the force P, is assumed. Theoretically, at the edges of the body infinite contact pressures are obtained [11]. The pressure distribution at the interface of the two bodies can be described as

$$p(x) = \frac{P}{\pi} \frac{1}{\sqrt{b^2 - x^2}} \tag{9}$$

and can be seen in Figure 13. The theoretical stress is limited by the material's yield stress σ_Y, resulting in a "plastic zone". [17]

For nominally flat surfaces, the pressure distribution across the contact length will be uneven [11]. The mean pressure is given by

$$p_{\mathrm{m}} = \frac{P}{2b} = \frac{\pi p(x=0)}{2}. \tag{10}$$

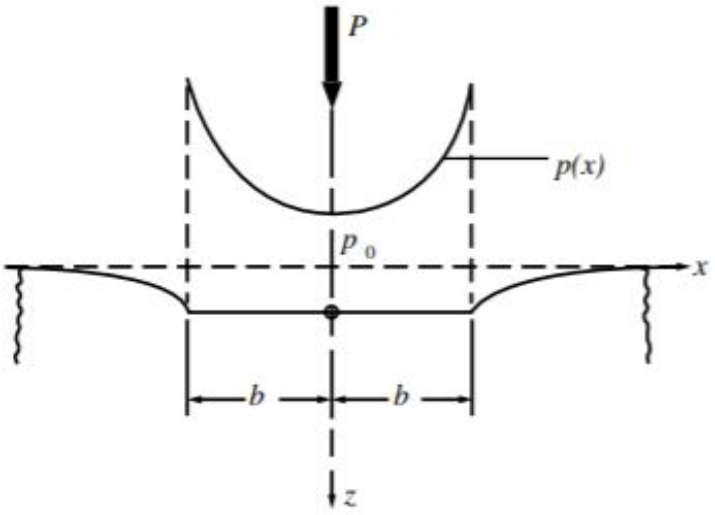

Figure 13: Contact between a flat punch and an elastic half space [11].

Typically manufactured surfaces are not completely flat, neither on a macroscopic nor on a microscopic scale. Macroscopic deviations are recorded by the flatness. Even for macroscopically flat surfaces the contact will only occur at discrete contact

spots due to the surface roughness. The real contact area is a composition of these small contact spots and will, even for high loads, be a fraction of the nominal area for most materials. [9]

For many applications it is critical to know the real contact area of two surfaces. Besides of many physical properties, the real contact area is crucial for static and dynamic sealing elements. The smaller the real contact area, the more leakage paths are available. The real contact area is dependent on material and surface properties and the contact pressure. Figure 14 shows that higher contact pressures lead to a higher contact area and fewer leakage paths. To describe the influences a basic understanding of contact mechanics on a microscopic scale is necessary. [18,19]

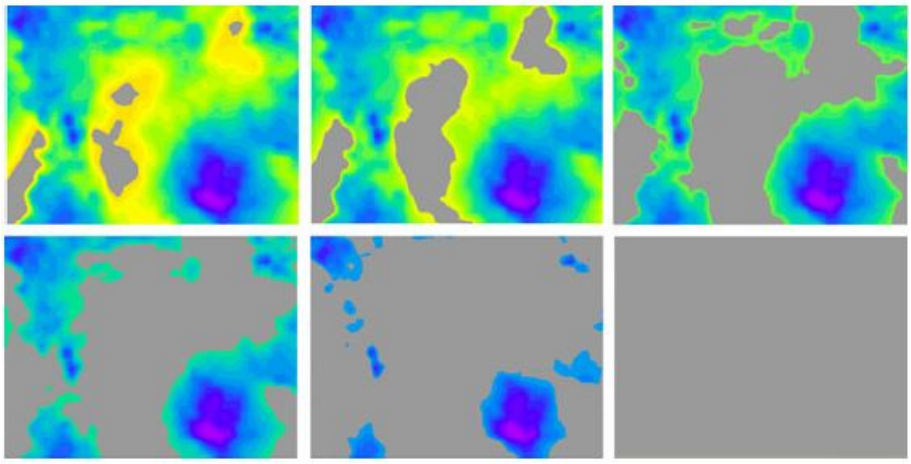

Figure 14: Influence of an increase of the contact pressure on the real contact area. The area that is in contact is greyed out [18].

The Hertzian contact model between a rigid sphere and an elastic half space can be used to describe various problems. On a macroscopic scale the Hertzian theory cannot be used for a flat punch. Nonetheless, this theory is essential if the contact of rough surfaces is viewed on a microscopic scale. Most elastic contact models are based on this principle. [18, 19, 20]

The Greenwood-Williams theory is one of the simplest models to describe the elastic contact between a randomly rough surfaces without friction and is still often referenced. The detailed mathematical derivation and further details can be found in Popov [18]. To simplify the problem, one of the surfaces is assumed as perfectly flat. The second surface, called effective surface, can be seen as a combination of the two real surfaces in contact. This effective surface consists of spherical bumps with equal radii R_p. Their height is statistically distributed with a standard deviation of σ_p. The representation of both surfaces can be seen in Figure 15.

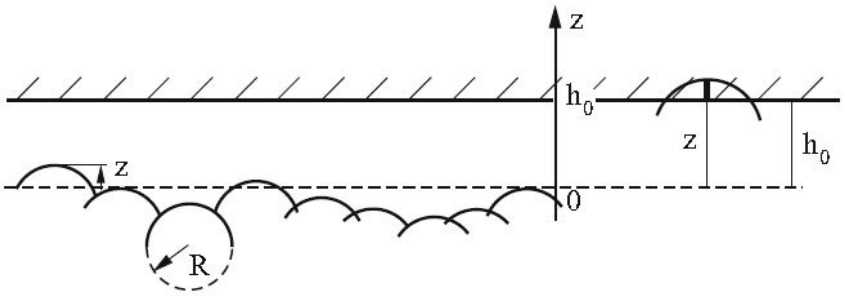

Figure 15: Model of the two contact surfaces according to the Greenwood-Williams theory [19].

The effective elastic modulus is defined as

$$E^* = \left[\frac{1-\nu_1^2}{E_1} + \frac{1-\nu_2^2}{E_2}\right]^{-1}, \tag{11}$$

where ν_1, ν_2 are the Poisson's ratios and E_1, E_2 the elastic moduli of the two actual bodies that are in contact. The curvature of the peaks of the effective surface R_p is calculated as

$$\frac{1}{R_\mathrm{p}} = \frac{1}{R_\mathrm{p1}} + \frac{1}{R_\mathrm{p2}}, \tag{12}$$

where R_p1 and R_p2 are the radii of the peaks of the two surfaces. Similarly, the effective standard deviation of the peak-height distribution σ_p is obtained by

$$\sigma_\mathrm{p}^2 = \sigma_\mathrm{p1}^2 + \sigma_\mathrm{p2}^2, \tag{13}$$

where σ_p1 and σ_p2 are the standard deviations of the height distribution of the two surfaces in contact. [9]

It is assumed that the asperities in contact are not influencing each other. Therefore, the asperities in contact have to be distant to each other, which is only true if the real area of contact is small compared to the nominal area. For this assumption the contact between the two surfaces can be seen as a number of Hertzian contact pressings, and the real area of contact can be calculated by integration over all surface heights that are in contact. The actual number of asperities that are in contact is determined by the mean separation h of the surfaces. The total number of touching asperities, the contact surface and the total needed force increase exponentially when reducing the separation h. [18] The ratio between the real contact surface A_r and needed total force F_N can be described as

$$\frac{A_\mathrm{r}}{F_\mathrm{N}} \approx \left(\frac{R_\mathrm{p}}{\sigma_\mathrm{p}}\right)^{1/2} \frac{3.2}{E^*} \approx \frac{1}{R_\mathrm{dq}} \frac{\kappa}{E^*}, \tag{14}$$

where E^* is the equivalent elastic modulus and R_dq the root mean square (RMS) slope of the surface profile. κ is a coefficient that is slightly dependent on static

properties of the surface and is around 2. As the radii of the asperities are not constant and they are not easily measured, the roughness parameter R_{dq} can be used for approximation. [18]

Usually leakage is prevented, when the asperities are squeezed by half. The needed stress can be approximated as seen in Equation 15. As R_{dq} is scale-dependent, so is the needed stress. With higher resolutions of the surface analysis methods, smaller asperities can be detected, so that the root mean square slope of the profile will increase. Although seals might not leak on a macroscopic scale, leakage paths on smaller scales are still present. The leakage flow is decreasing exponentially with an increase of the contact pressure. [18]

$$\sigma_{\mathrm{seal}} \approx \frac{1}{4} E^* R_{\mathrm{dq}} \tag{15}$$

The effect of non-Gaussian surfaces has been investigated by Kotwal and Bhushan [21]. The influence of skewness and kurtosis on the area of contact can be seen in Figure 16. The real contact area is decreasing with an increase in kurtosis, and the optimum skewness is around 0 to 0.5, varying on the contact pressure. [9, 21]

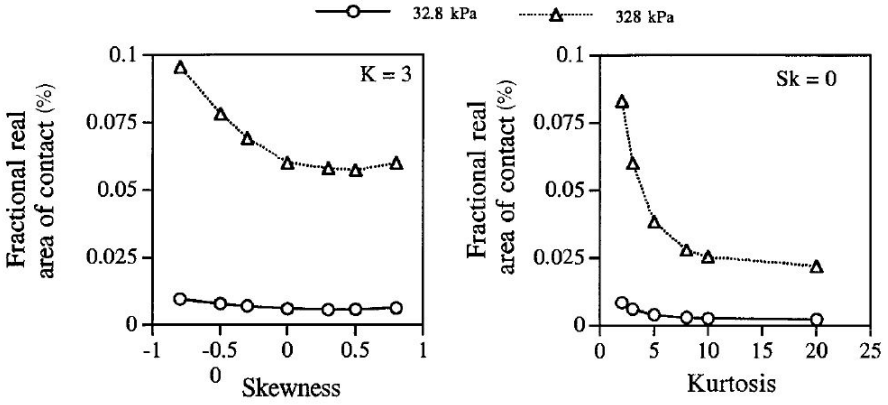

Figure 16: Influence of skewness and kurtosis on the real contact area at applied pressures of 32.8 and 328 kPa ($E^* = 100$ GPa) [9].

The models shown above are all based on elastic deformation of the asperities. As the real contact area is rather small, the stresses in the regions touching are relatively high. Materials like steel that might be loaded in a range, where only a purely elastic deformation is expected on a macroscopic scale, are likely to deform plastically on a microscopic scale. Greenwood and Williams introduced a plasticity index ϕ to estimate the degree of plastic deformation. [9, 18] It can be calculated as

$$\phi = \frac{E^* R_{\mathrm{dq}}}{H}, \tag{16}$$

where H is the surface indentation hardness of the softer material in the unit of the effective modulus. This surface hardness is different from the bulk hardness and is not easily measured. [9] Common approximations of the used hardness can be found

in literature [9, 20, 22, 23, 24]. Cook and Bhushan [22] experimentally established, that the ratio between the surface and bulk hardness can be assumed as 2 for metals. Tabor [23] shows that for metals and non-metals the hardness can be estimated as three times the yield strength. Plastic flow will occur when $\phi > 1$, whereas when $\phi < 0.6$ the main mechanism is elastic deformation. [9] The plasticity index can be derived from the normal separation of the two surfaces, when the asperities in contact start deforming plastically. The derivation can be found in Bhushan [9].

When plastic deformation occurs, the problem can be seen as a hardness indentation. Bowden and Tabor [25] introduced an estimation for the real contact area, which is shown in Equation 17. This very simplified model assumes that the pressure in a single asperity in contact is only dependent on the hardness of the softer material and not on the surface roughness. Therefore, the real area of contact increases linearly with the applied normal force, and other surface characteristics are not considered. [9,18,20] Additionally, the usage of the surface hardness comes with the above discussed uncertainties, so that this equation will give a rough estimation for the real contact area at best.

$$\frac{A_\mathrm{r}}{F_\mathrm{N}} \approx \frac{1}{H} \tag{17}$$

3.3 Fractal Based Contact Mechanics

The introduced contact mechanics theories have certain limitations. It is assumed that the asperities in contact do not influence each other. This is only the case for real contact areas that are a fraction of the nominal one. Another problem is the scale dependency of surface roughness. A higher resolution of the measurement device will result in the detection of an even smaller scale of roughness. The contact mechanics theory by Persson [26,27] eliminates these two factors, therefore no length scale of surface roughness is excluded from the analysis. Figure 17 shows a rubber block pressed against a hard solid on different length scales.

The real area of contact $A(\zeta)$ is a function of the length scale $\lambda = L/\zeta$ that is analysed, where L is the order of the contact length and ζ is the magnification. The function $P(\zeta) = A(\zeta)/A(L)$ is studied. Note that $P(\zeta = 1) = 1$, and $A(L) = A_0$ which is the nominal contact area. The stress distribution at the magnification ζ is given by the function $P(\sigma, \zeta)$. The inputs necessary for this theory are the power spectral density $C(q)$ and the elastic properties E and ν of the two contacting bodies. [26, 27, 28] The functions for the stress distribution and real contact area are rather complex. Their derivation and complete form for self-affine fractal surfaces can be found in Persson [27]. Similar to the Greenwood and Williams model, Persson predicts a linear increase of the real contact area for small loads. This can be seen in Figure 18, which also shows the dependency of the normalized contact area on the magnification. At higher loads the real area of contact increases, more asperities are in contact and the asperities are not distant to each other any more. The interaction of asperities plays a significant role, resulting in a smaller increase of the real surface area with higher loads. [26,27,28]

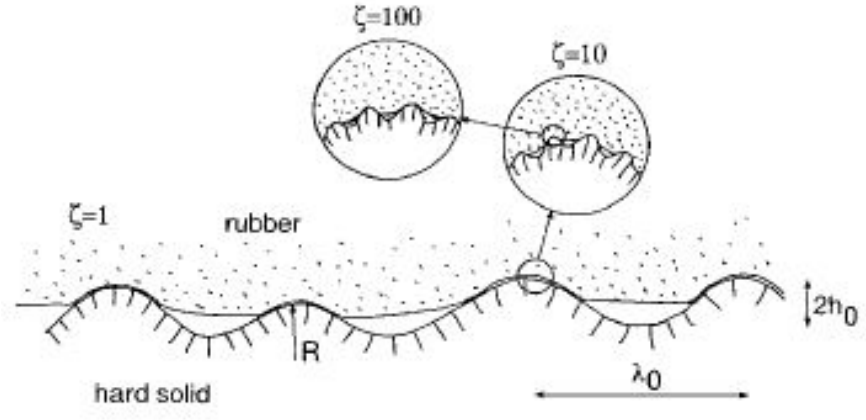

Figure 17: Contact of two self-affine surfaces on multiple length scales (magnifications $\zeta = 1$, 10 and 100) [27].

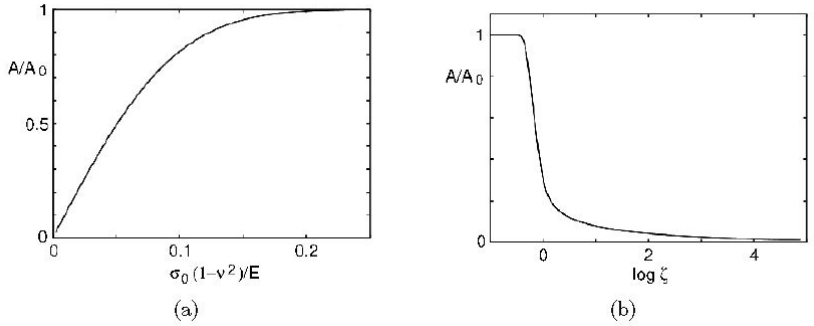

Figure 18: Influence of (a) the squeezing pressure and (b) the magnification on the normalized real contact area [28].

This contact model can be extended for elastoplastic contact and the derivation can be found in Persson [26]. The further discussed fractal leakage models are based on this contact theory.

To expand the fractal contact mechanics to viscoelastic materials further adaptations have to be made. The area of contact for each asperity, which is in contact with the counter surface, will increase over time when the applied contact pressure stays constant. The broad distribution of relaxation times for polymers will lead to an increase of the real contact area over a long period of time t. To generalize the above discussed contact mechanics, the moduli of the surfaces in contact have to be replaced by the viscoelastic modulus $E(t)$. All functions describing the real area of contact and stress distribution are therefore additionally dependent on the time [29]. The further discussed leakage models do not take this effect into account.

3.4 Modelling Leakage

Most simple leakage models assume that the leakage flow can be described as a laminar flow through an annular gap. In case of a circular seal the total volumetric flow rate can be calculated as

$$Q = \frac{2\pi h^3 (p_i - p_0)}{12\eta \ln \frac{r_0}{r_i}}, \tag{18}$$

where h is the mean separation between the two surfaces, $(p_\mathrm{i} - p_0)$ the pressure drop across the seal, η the dynamic fluid viscosity and r_0 and r_i the outer and inner diameter. [9] Bhushan [9] proposes that for elastic contacts the mean separation can be calculated as

$$h = \sigma_\mathrm{p} 1.4 \left[\frac{0.57(nR_\mathrm{p}\sigma_\mathrm{p})E^*(\sigma_\mathrm{p}/R_\mathrm{p})^{1/2})}{p_\mathrm{c}} \right]^{0.65}, \tag{19}$$

where n is the density of asperity summits per unit area and p_c the apparent contact pressure.

More recently developed leakage models, like the ones developed by Persson [30] and Zhang [31] are based on the principles of fractal contact mechanics. The basics of the critical constriction leakage theory [28, 30, 32, 33], which was developed by Persson and his colleagues, is discussed in the following. It uses the power spectral density, which was introduced in Chapter 3.1 (Figure 11), to describe the influence of surface roughness on the frictional properties on all length scales. Similar as discussed in Chapter 3.3 the interface between the two bodies in contact is studied at different magnifications ζ. In this theory a rectangular seal with an area $L_\mathrm{x}\mathrm{x}L_\mathrm{y}$ is divided into $N = L_\mathrm{y}/L_\mathrm{x}$ squares with the side length of $L_\mathrm{x} = L$. This can be seen in Figure 19.

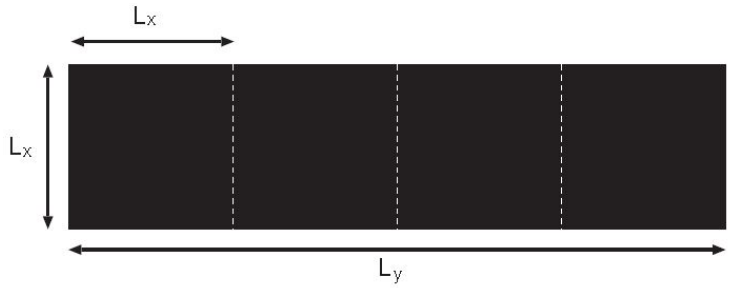

Figure 19: Theoretical contact area of the seal [30].

Furthermore, only one of those squares is considered. On a macroscopic scale, where the magnification $\zeta = 1$, the contact between the two bodies seems complete. With higher magnifications interfacial roughness can be detected and the contact area will decrease. Once the magnification is high enough a continuous percolation path is observed. At this critical magnification ζ_c, the lateral size of the most narrow constriction is $\lambda_\mathrm{c} = L/\zeta_\mathrm{c}$. The process of increasing the magnification and the critical

constriction along the percolation path can be seen in Figure 20. At the critical magnification the separation between the two surfaces is $u_1(\zeta_c)$. When the magnification is further increased, more percolation channels are observed, but their most narrow constriction is smaller than the one observed at the critical magnification. [30]

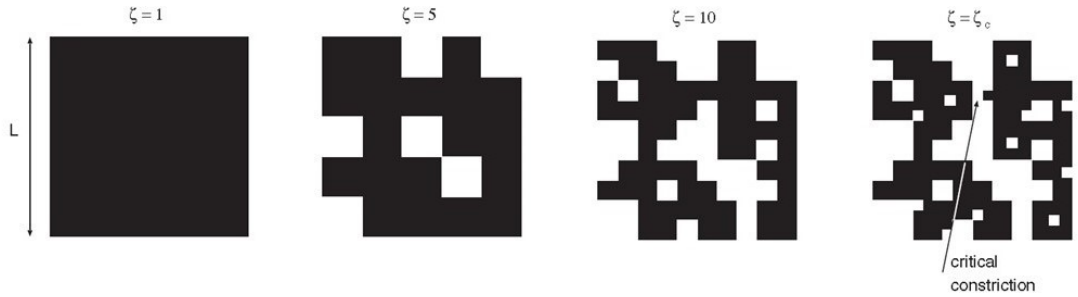

Figure 20: Principle of increasing the magnification ζ until the critical constriction ζ_c is reached [30].

The critical constriction theory assumes that all leakage occurs at the critical percolation channel, and the whole pressure drop ΔP occurs at the critical constriction. For an incompressible Newtonian flow the volume flow through one considered square is given by the Poiseuille flow shown in Equation 20.

$$Q = \alpha \frac{u_1^3(\zeta_c)(p_i - p_0)}{12\eta}. \tag{20}$$

As the exact shape of the critical constriction is not rectangular, a correction factor α can be introduced. The real flow channel is not rectangular, but its pore height decreases to zero at the edges. Therefore, it is expected that $\alpha < 1$. The leakage through the whole seal is obtained by multiplying the leakage through one square by the total number of squares N.

Lorenz [28] validated the above theory by comparing it to experimental measurements. The exponential decay of the leak rate with an increasing squeezing pressure can be seen in Figure 21. For fluid pressures that are much smaller than the prevalent contact pressure ($p_a << p_c$) the model predicts a linear relation between the leak rate and the fluid pressure. Lorenz proposes that once the fluid pressure reaches about 60% of the contact pressure its influence on the contact mechanics cannot be neglected any more. On the high pressure side the seal ring will start to lift off and the measurement becomes unstable. This phenomenon can be included into this theory. Figure 22 shows the comparison of the experiment to the theory.

When not only the leakage through the critical junction, but the leakage through the whole interface is considered, a new concept has to be introduced. Zhangs [31] model replaces the sealing interface with a representative one-layer porous medium and its properties can be calculated for elastic, elastic-plastic and plastic contact. A theoretical permeability K_ν can be assigned to the porous interface. It is dependent

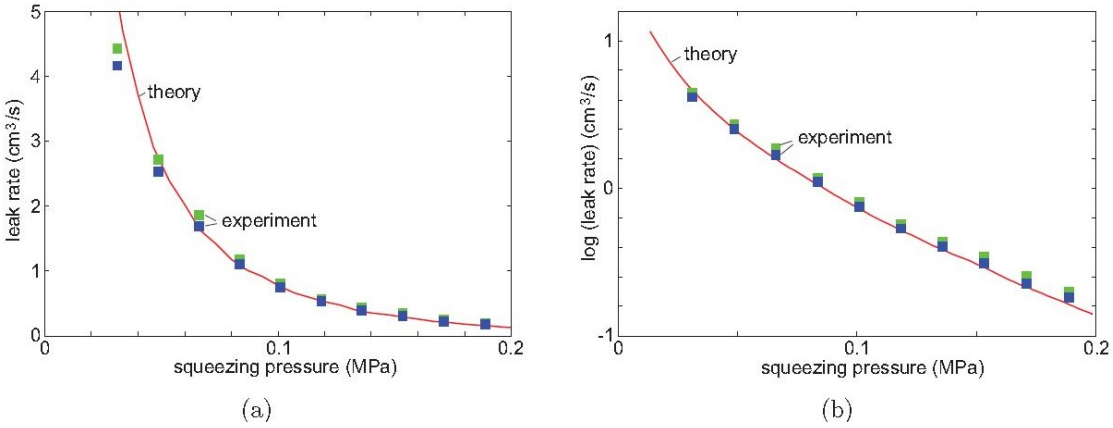

Figure 21: Influence of the squeezing pressure on the leak rate [28].

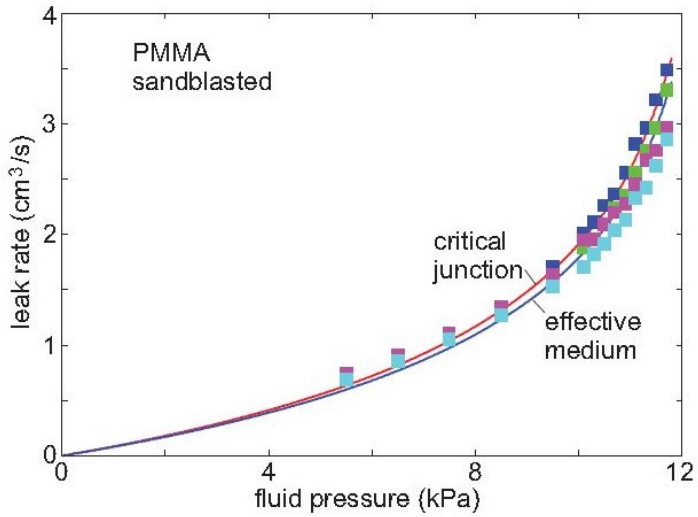

Figure 22: Influence of the fluid pressure on the leak rate [28].

on the fractal properties, material parameters, the geometry of the interface and the contact load. The leakage for a ring gasket can be calculated as

$$Q = \frac{2\pi K_\nu h_\mathrm{c} \left(p_\mathrm{i} - p_0\right)}{\eta \ln \frac{r_0}{r_\mathrm{i}}}, \tag{21}$$

where h_c is the vertical height of the percolation channels, which is also a function of the fractal properties, the elastic properties and the contact load. Again, this model predicts linear increase of the leakage with an increasing pressure differential for gas pressures significantly smaller than the contact pressures and a logarithmic decrease with increasing contact force. Zhang [10] validated this model experimentally. The dependencies of the leakage on the contact force and the applied gas pressure can be seen in Figure 23.

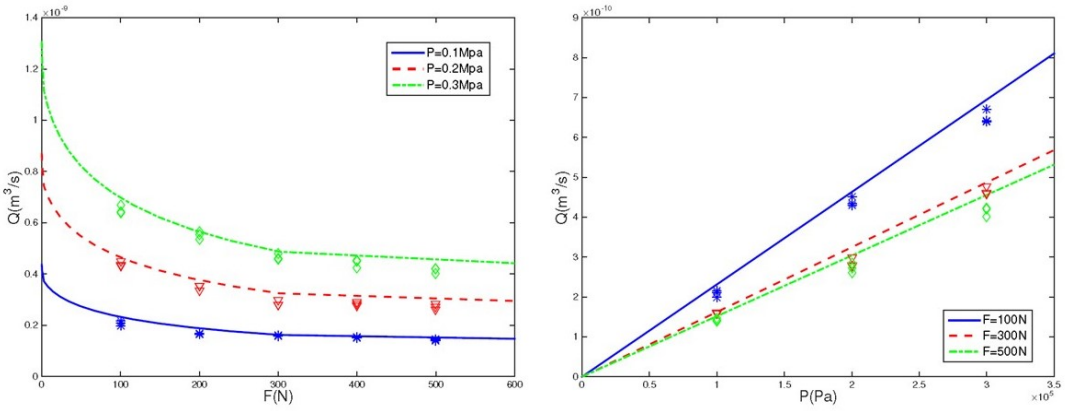

Figure 23: Influence of the contact force F (left) and the fluid pressure P (right) on the leak rate. (lines...calculated flow rate, data points...experimental flow rate) [10].

3.5 Other Parameters Influencing Leakage

There are plenty of other parameters that have an impact on the sealing and that have not been discussed. Operating temperatures, environmental influences and the gas type are just some of those [34]. Only factors that are also present at the experimental setup are discussed further.

The properties of viscoelastic materials are time dependent and consequently the deformation of the asperities in contact is changing over time as well. The time that the surface pressure is applied for is influencing the actual surface area. The real contact surface is increasing over time [32]. Persson [29] includes this effect in his contact theory, but it is not included in the discussed leakage models. As the asperities are further deformed with time, the size and shape of the leakage channels will change and the mean separation of the surfaces will decrease. The mean separation at the critical magnification $u_1(\zeta_c)$ is time dependent, resulting in a time dependent leakage (cf. Equation 20). Similar to this the viscoelastic properties could be taken into account in the leakage model, developed by Zhang [31]. The introduced permeability K_ν and the vertical height of the percolation channels h_c depend on the modulus of the materials. This results in a time dependent leakage model.

Not only the reversible viscoelastic properties, but also irreversible plastic deformations have an impact on the leakage. Figure 24 shows the influence of the predeformation on the leakage. Flitney [34] ran tests with loading and unloading cycles. Once the contact pressure is reduced the flow rate is not getting back to its original value. This is due to the viscoelatic and plastic properties of the materials. When the contact pressure is reduced, it takes time for viscoelastically deformed asperities to deform back to their original state. During this process the leakage increases slowly. As these viscoelastic processes are reversible, they will always take place. If no plastic deformations occur, the material will go back to its original state after a

sufficient amount of time. Plastic deformations of the asperities are not reversible. When the contact pressure is reduced the asperities will not deform back. Once a seal is loaded in such way, that plastic deformation occurs, it will not behave like the original one. This viscoelastic behavior and the dependency on predeformation are not included in the discussed leakage models.

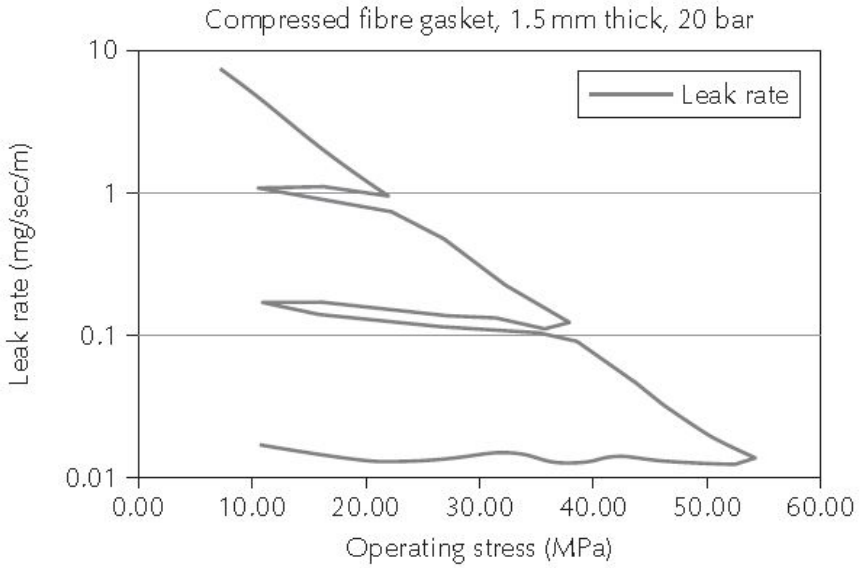

Figure 24: Influence of the contact pressure on the leakage rate for loading and unloading cycles [34].

Contamination and impurities on the interface of the seal are very problematic, as their magnitudes are often lager than the surface roughness. Bauer [24] finds, that leakage rates for lapped surfaces are smaller than for turned ones, as the surface roughness is reduced in lapping. When both surfaces are contaminated the leakage is identical, although the original surface texture is different. Especially for low contact pressures contamination can cause huge problems.

4 Experimental

This chapter describes all relevant information regarding the test equipment, the test setup and the manufacturing of specimens. The used materials and important material parameters are presented. Furthermore the characterized specimen parameters and the design of experiments are introduced.

4.1 Test Rig

In the application, the contact pressure is dependent on the pressure differential in a packing case as discussed in Chapter 2.4. The test rig should resemble the application as well as possible and only one leakage path should be present. In cut rings multiple ones are available. Uncut sealing rings with only one possible leakage path through their contacting surfaces were used. A test rig design, where an independent application of contact pressure and gas pressure is possible, is necessary. In order to function properly the test rig has to meet the following requirements:

- The test rig needs to allow a defined application of the nominal contact pressure. If the nominal contact area is known, an according force can be used to achieve the desired contact pressure.
- To ensure that contact happens at the desired location the rings need to be centered.
- The application of the gas pressure has to be independent of the contact pressure application. Additionally, it must be possible to set a range of gas pressures.
- Leakage is only allowed through the interface between the two sealing rings. All other leakage paths in the pressure chamber have to be prevented.
- The leakage through the sealing rings has to be measured. This can be done in the pressure line or afterwards without counter-pressure.

Based on the above requirements a test rig was developed. Special thank goes to Christian Gollmann, who drew the test rig design. Figure 25 shows the flow chart as well as a picture of the test arrangement. A defined compressive force is applied by a tensile testing machine. The tensile testing machine used is a RetroLine testControl II AllroundLine 1474 (Zwick Roell, Germany) with a load cell type KAF-W 10kN (A.S.T. GmbH, Germany). To compensate tilting of the test rig, a pressure plate with a ball joint is used on one side.

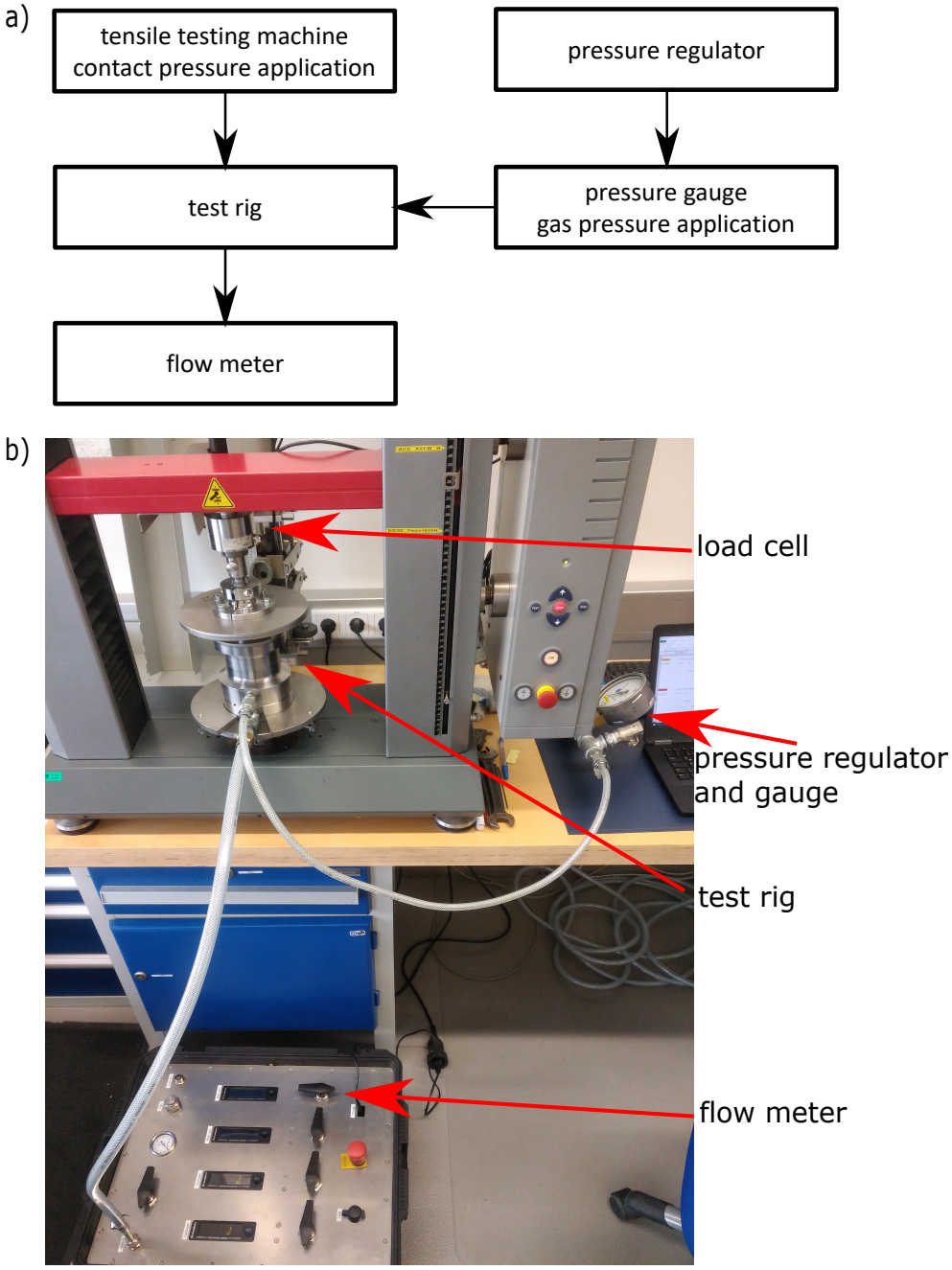

Figure 25: Flow chart (a) and picture (b) of the test arrangement showing all the used equipment.

Figure 26a shows a cut through the test rig. A constant force, resulting in a defined nominal contact pressure at the interface of the two sealing rings, is applied. A gas pressure, which is regulated by a gas control valve, can be introduced into the system. It is assumed, that the pressure drop in the gas supply line is neglectable, which is true for sufficiently large pipe diameters. Therefore the gas pressure in the pressure chamber p_a is equal to the reading of the gas pressure measurement. O-rings reduce unwanted gas leakage and the green marked leakage path through the

sealing rings is dominating. The smaller sealing ring facing the rod is called stamp ring (SR) and the larger ring facing the mountable cover is called cover ring (CR). Small unwanted leakages through the O-rings are not influencing the measurement as long as the leakage flow measurement is not done in the pressure line, but afterwards and as long as they are small enough to not cause a pressure drop in the pressure chamber. The leakage flow measurement is done with a MASS–VIEW® meter MV102 or MV106 (Bronkhorst High-Tech B.V., The Netherlands), depending on the amount of leakage.

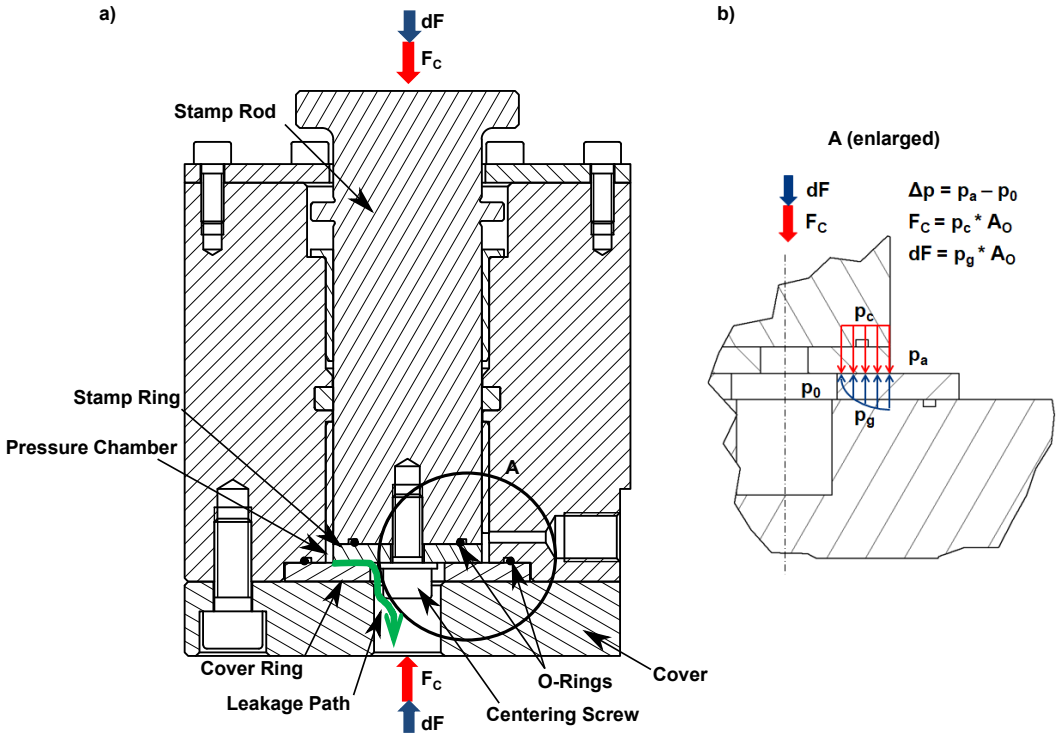

Figure 26: Cut through the test rig (a) and the resulting simplified pressure situation (b).

A more detailed, but still simplified view of the pressure situation at the sealing interface is shown in Figure 26b. The applied force F_C results in a nominal contact pressure p_c. In the pressure chamber a pressure of p_a is applied. The surface roughness of the two sealing rings results in small gaps and allows the gas to creep inside the interface. A gas pressure profile $p_g(r)$ as discussed in Chapter 2.4 occurs, which is a function of the radius. As the traverse of the tensile testing machine is locked, an additional force dF is necessary to keep the traverse at the same position. This force can be measured and is equal to the integral of the pressure profile p_g multiplied with the nominal contact area A_0.

A detailed discussion about the advantages and disadvantages and an analysis of fault effects can be found in Chapter 5.1.

4.2 Test Specimen

A top view and the diameters of the rings are shown in Figure 27. It also shows the outer $d_{\mathrm{o,CR}}$ and inner $d_{\mathrm{i,CR}}$ diameter of the cover ring, as well as the outer $d_{\mathrm{o,SR}}$ and inner $d_{\mathrm{i,SR}}$ diameter of the stamp ring. The nominal contact surface and the sealing length of the interface are controlled by the inner and outer diameters of the two sealing rings in contact. A thickness of 5 mm was chosen for the sealing rings, which is about the thickness of typical packing rings. 10 mm was chosen as a standard sealing length, which is the result of $(d_{\mathrm{o,SR}} - d_{\mathrm{i,CR}})/2$. To investigate the influence of the sealing length, it was reduced to 7.5 and 5 mm by increasing the inner diameter of the cover ring $d_{\mathrm{i,CR}}$.

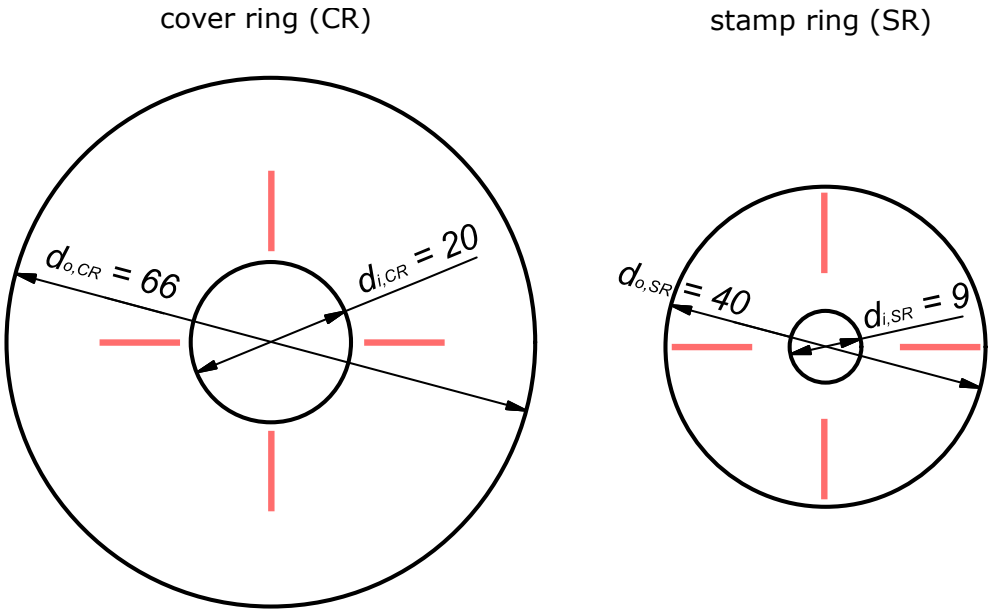

Figure 27: Dimensions of the sealing rings in mm. The locations of the roughness measurements are marked red.

4.3 Used Material

In this section the investigated materials are introduced. In the application various leakage paths can occur as described in Chapter 2.5. Leakage without relative motion can occur through the joints of cut rings, two sealing rings, a sealing ring and a backup ring or the face of a cup. Based on those combinations the following material pairs have been chosen for leakage studies:

- sealing ring material and steel (resembling sealing ring and cup)
- sealing ring material and bronze (resembling sealing ring and backup ring)
- a sealing ring material with another sealing ring material (resembling two sealing rings and the joints of ring segments)

- bronze and steel (resembling the backup ring and cup)

Two frequently used HOERBIGER packing ring materials, one PTFE based and one PEEK-based, were chosen as polymeric sealing ring materials. The components of the PTFE based HY54 grade and the PEEK based HY103 grade can be seen in Table 1. Detailed compositions are crucial advantages over competitors and can therefore not be disclosed.

Table 1: Basic components of the used Hoerbiger HY grades

HY54	**HY103**
PTFE	PEEK
Carbons	PTFE
Glass Fibers	Carbons
	Carbon Fibers
	Molybdenum disulfid

Bronze, which is typically used for backup rings, and martensitic steel X20Cr13, which is often used for cups, are chosen as additional sealing ring materials. Table 2 shows an overview over relevant material properties of HY54, HY103, bronze and steel.

Table 2: Overview over mechanical properties of the used materials.

Property	**HY54**	**HY103**	**Bronze**	**Steel**
Tensile Strength (MPa)	≥ 17.2	≥ 50	~ 400	~ 700
Elongation at Break (%)	≥ 74.9	≥ 1.7	~ 15	~ 13
Tensile Modulus (MPa)	1439 ± 272	4408 ± 962	~ 110000	~ 210000
Shore D Hardness	63.3 ± 4.2	81.1 ± 3.3		
Brinell Hardness (HB)			~ 120	~ 220

4.4 Manufacturing Methods

Specimens with differently manufactured surfaces were produced. Relevant methods are turning, (hand) grinding and fine grinding. Table 3 shows all used devices to manufacture the specimens and their surfaces. The methods used for each material are based on the typical manufacturing of packing components. The geometry of polymeric packing rings and backup rings is usually turned and milled. For polymeric packing rings the surfaces are hand grinded to achieve a finer finished surface. The hand grinding was performed with sand paper with an ISO grit size of P180 for the coarse hand grinding and P320 for the fine hand grinding. Backup rings, made of bronze, are usually fine grinded and the steel cup faces are surface grinded.

Table 3: Used machines for manufacturing the specimens and its sealing surface.

	Machine	Manufacturer
Polymer Turning	Quick Turn Nexus 200-II MY	Mazak, Japan
Metal Turning	Integrex j-200S	Mazak, Japan
Steel Grinding	Kehren D10	Kehren GmbH, Germany
Bronze Grinding	AC microLine 700-F	Lapmaster Wolters GmbH, Germany

In order to examine different surfaces the turning parameters are adapted so that different surfaces are produced. Fetecau [35] finds that for turning polytetrafluorethylene the feed rate is a parameter that influences the surface roughness. An increase of the feed rate leads to a higher surface roughness. Additionally the grinding sand paper grit size was varied. The used turning parameters can be found in Table 4. Based on them the design of experiments, which is discussed in Chapter 4.6, was selected.

Table 4: Used machine parameters for manufacturing the specimens and their sealing surfaces.

	Feed Rate (mm/U)	**Cutting Speed** (m/min)	**Depth of Cut** (mm)
Polymer Turning (fine)	0.05	300	0.5
Polymer Turning (coarse)	0.08	300	0.5
Metal Turning	0.1	200	0.5

4.5 Specimen Characterization

As the influence of the sealing surface is of interest, the manufactured surfaces were characterized. The original focus of the investigation lies on the influence of the surface roughness. It is attempted to hold the influence of the larger scale surface deviations, such as flatness, to a minimum. Still both sides of the sealing rings were scanned with a coordinate-measuring machine type LH 65 (Wenzel, Germany) to get feedback of the amount and scatter of larger scale surface deviations.

The surface roughness was measured according to DIN ISO 1302 and the in Chapter 3.1 introduced roughness parameters were recorded. The power spectral density is not measured, as measurements on multiple length scales are necessary. The used profilometer type is Hommel etamic T8000 RC (Jenotptik, Germany). Surface roughness measurements were performed radially outwards along the sealing length on four locations to get information about the deviations on a single part as well. This is shown in Figure 27. Measurements in tangential direction were not performed, because they are inconclusive for face turned rings.

4.6 Design of Experiments

A simple design of experiments was chosen to accommodate all areas of interest. The influence of manufacturing was included by using different methods and changing their parameters. As the different manufacturing methods result in different surfaces in terms of roughness and other surface parameters, not only the manufacturing method influence can be studied, but also the influence of the surface deviations themselves. For each material pair, as discussed in Chapter 4.3, eight possible combinations were tested, see Figure 28. The same procedure was performed for the PEEK based material grade HY103. For the combination of bronze and steel only four variations were tested. A turned and a grinded bronze part was tested against a turned and a grinded steel ring.

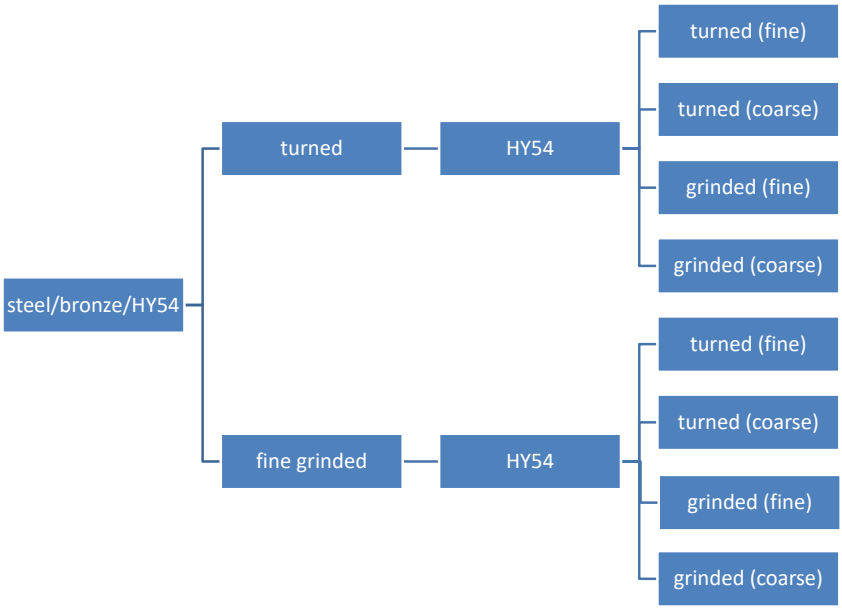

Figure 28: Performed design of experiment on the example of HY54. The stamp rings are made out of HY54 and the cover rings material is varied.

4.7 Testing Process

All measurements were performed with following environmental surroundings, which differ slightly from the standard atmospheres for plastics defined in DIN EN ISO 291: The room temperature is kept constant at 20 ± 1 °C and the relative humidity at 50 ± 5 %. All specimens are stored at the same conditions for at least 24 hours prior to testing.

In order to achieve valid results the following testing procedure has to be met:

- *Test Rig Assembly*: The test rig has to be assembled as shown in Chapter

4.1, so that the leakage measurement takes place end-of-line without counter-pressure.

- *Sealing rings insertion*: The sealing surfaces must not contain dirt or other foreign objects. After machining the surfaces are blown off with compressed air. Before the testing, the surfaces need to be visually checked for foreign objects. Any visible objects need to be removed. Once the surfaces are clean, the stamp ring has to be inserted and fixed with a screw, so that it stays centered. Then the cover ring can be inserted. The intended sealing surfaces must face each other. The cover has to be put on last and fixed with three M10 screws and a torque of 10 Nm. Figure 26 shows the finished assembly.

- *Test program*: A standard test program has been created. Once the test rig is assembled, the traverse can be run to the starting position, where there is no contact between the upper pressure plate of the tensile testing machine and the stamp rod of the test rig. The force has to be zeroed out at this position. To ensure a smooth clamping first the traverse compresses until a pre-force of 30 N is reached, then it runs further with a defined velocity until the desired normal force, which is defined by the desired contact pressure, is reached. The contact force is held for five minutes to compensate the largest part of polymer relaxation. After this holding time, the control is switched to a position controlled hold of the traverse. Now the gas pressure can manually be raised step by step from zero to 10 bar gauge pressure. The force that is necessary to hold the traverse at its position will increase with increasing gauge pressure. First, the leakage will increase until an equilibrium is reached. After that, the leakage starts to drop again due to relaxation and creeping of the viscoelastic polymer. The recorded leakage value is the peak value before this decrease of the leakage. Once all pressure levels are recorded, the pressure has to be set to zero again and the traverse is run to the starting position once again. A new higher contact pressure level can be set and the measurement program can be run again.

The nominal contact pressure at the sealing interface is set to 2, 3, 5, 7, 10, 15 and 3 bar. It is important that lower pressures are measured first to minimize the influence of predeformation of the polymeric specimen. After the highest pressure, again a contact pressure of 3 bar is set again to investigate the influence of predeformation. Air is used as a gas for all performed tests.

A recorded force against time diagram is shown in Figure 29, where all elements of the test program can be seen. First the sealing rings are loaded with a force, according to the desired contact pressure. After a five minute holding time, the gas pressure is increased, which results in an increase of the force needed to hold the traverse in its position. This additional force is further called $\mathrm{d}F$ and can be obtained by subtracting the initial force necessary to reach the desired contact pressure. For each gas pressure level the leakage Q and the total applied force F is recorded.

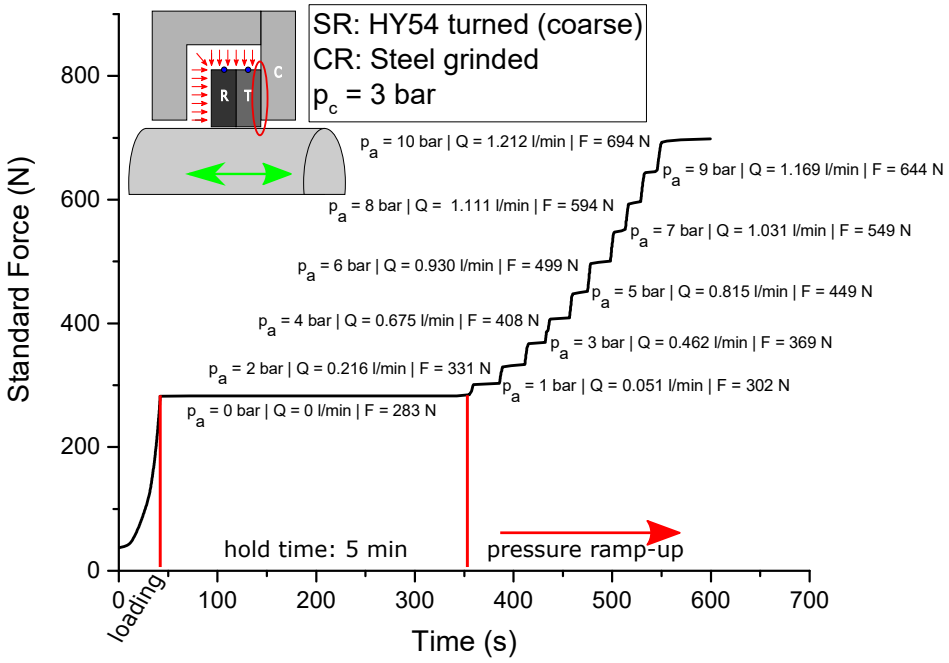

Figure 29: Used test program on the example of a contact pressure p_c of 3 bar.

5 Results and Discussion

This section presents all specimen properties and discusses the influence of the manufacturing on the finished surface. It describes the development of the testing procedure, the occurring problems and the minimizing of their influence. The testing procedure is analysed and the results from the conducted design of experiments are analysed.

5.1 Testing Procedure Development and Fault Analysis

In order to analyse the test rig with a simplified repeatability and reproducibility study, various factors have to be taken into account. The influence of important material properties and testing parameters on the testing procedure are discussed.

5.1.1 Viscoelasticity and Time Dependency of Leakage

The time dependency of mechanical properties is a typical characteristic of many polymers. This material behavior is caused by the morphology in plastics. Detailed mechanisms of creep and relaxation are not of interest in this thesis and are therefore not covered, but can be found in Ehrenstein [36].

The relaxation process does impact the test program. If immediately after applying a defined contact pressure the deformation is kept constant, the set force will decrease by about 10 %. Figure 30 shows that especially in the beginning this decrease is major. A normal force of 282 N equals a contact pressure of 3 bar. Once the desired force is reached, the traverse position is kept constant and the force starts to decrease. The nominal contact pressure decreases at the same ratio as well. In the application the nominal contact pressure is applied by the gas pressure itself and therefore stays constant. For meaningful results it is necessary that the contact pressure is known and kept relatively constant. Therefore a sufficient holding time of the specified force of five minutes was chosen to minimize the relaxation effect. Figure 30 also shows the importance of keeping vibrations and shocks to a minimum. Even little impact on the test rig leads to rearrangement of the asperities.

Once the deformation is kept constant measurement time is approximately four minutes. Because of the holding and the short measurement time the influence of relaxation can be neglected. Still, the long term leakage behavior is of interest, which is why a long term measurement was performed. After a five minute holding time a gas pressure of 3 bar was applied. Figure 31 shows that over time relaxation is still present and the force necessary to keep deformation constant decreases gradually. On a macroscopic scale the test can be seen as a typical stress relaxation test, which results in a decrease of the force. Processes on a microscopic scale at the interface result in changes of leakage. Figure 31 shows that over time leakage decreases as well. This effect implies that viscoelastic processes take place at the interface. It is believed, that at the interface the asperities creep and shift, so that the real contact area slightly increases and the size of leakage channels decreases. McFarlane [37]

showed that the surface area increases when the force is kept constant.

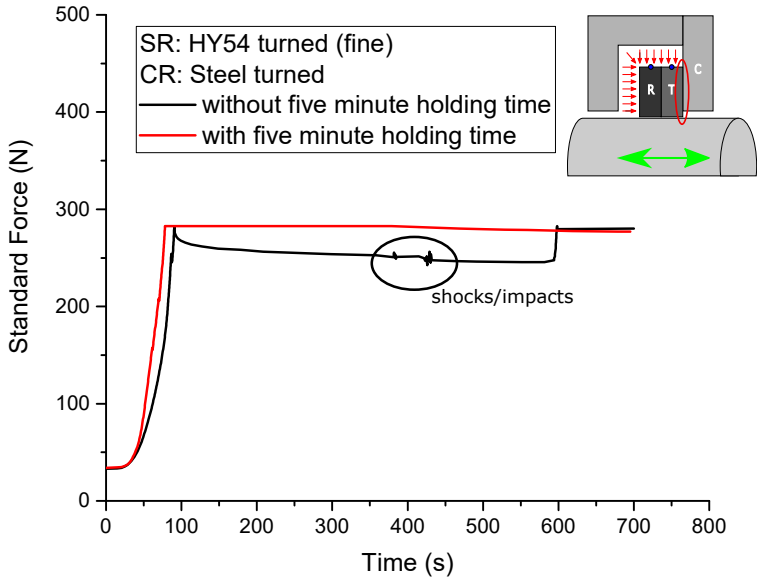

Figure 30: Influence of stress relaxation and introduction of a holding time.

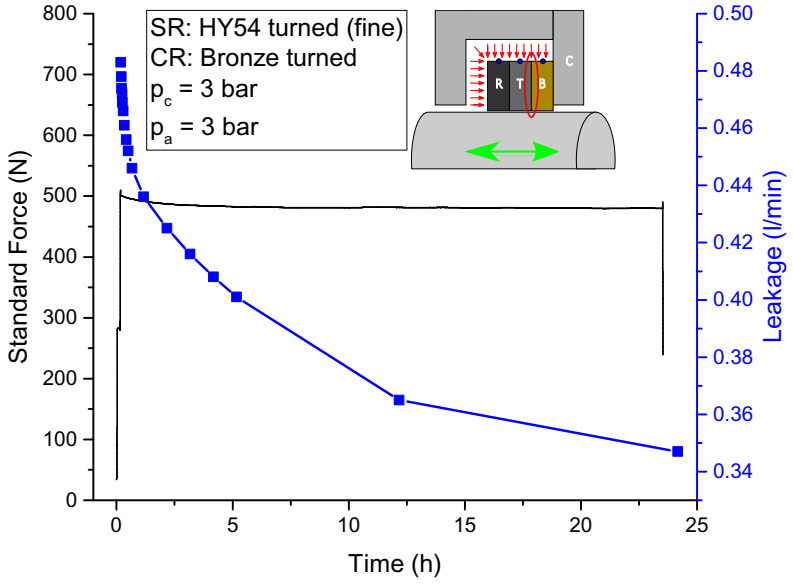

Figure 31: Influence of relaxation and creep on the necessary holding force and the leakage at long time (24 h) testing.

5.1.2 Predeformation Dependency

Increased contact pressures lead to an increase of asperity deformation at the sealing interface. Typical mechanisms for polymers are viscoelastic and plastic deformations. General information about deformation mechanisms in semi-crystalline polymers can be found in Ehrenstein [36]. Plastic deformations are irreversible while the viscoelastic deformation is reversible, but time dependent. As the modulus of steel and bronze is much higher than the one of the used polymer, it is believed, that the deformation of the polymer asperities is dominant and the influence of steel and bronze on the predeformation dependency can be neglected.

The time dependent viscoelastic deformation and the irreversible plastic deformation cause the predeformation dependency. Figure 32 shows a loading and unloading cycle of a sealing ring pair. Different contact pressures were applied. In between, the contact pressure was always reduced to 3 bar and the leakage was recorded. With higher predeformations, the leakage at a certain nominal contact pressure decreases. This is due to the irreversible and time dependent deformations of the mating surfaces, which result in higher real contact areas and smaller leakage channels. The time dependent viscoelastic deformations are reversible and after a sufficient amount of time these parts of the deformation reach their initial state. Their influence can be eliminated if the time between the measurements are long enough. Here the measurements were performed consecutively, therefore Figure 32 also includes viscoelastic influences.

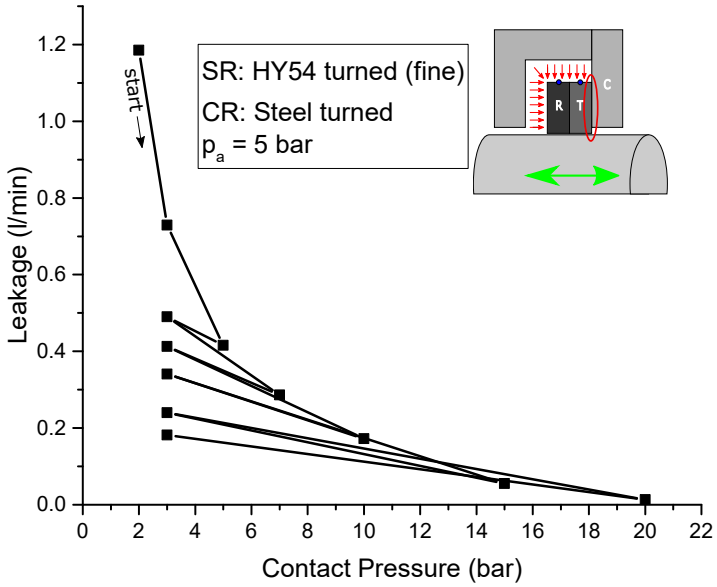

Figure 32: Influence of the predeformation on the leakage

The discussed leakage models do not take this influence into account. The dependency, found in this thesis, and the experimentally gained information by Flitney [34], which was discussed in Chapter 3.5, coincide qualitatively.

The measuring routine, as described in Chapter 4.7, tries to eliminate the influence of the vicoelasticity and the predeformation as far as possible. They would overlap with other influencing factors and are also not included in the theoretical models. The magnitude of the influence of the viscoelastic effects in the application is not easily estimated. One compression cycle is very short. The contact pressure is applied for a short period of time with a high frequency. These short loading times influence the material behavior as well, but are not considered in this thesis. Including those viscoelastic effects in discussed leakage models might help to further understand those processes.

5.1.3 Edge Pressure and Leakage Length Influence

As discussed in Chapter 3.2, the pressure distribution along a flat punch is not constant. This is evident at both edges of the leakage path. At the high pressure side of the ring pair, the edge of the polymeric ring is causing a pressure increase. At the low pressure side at the end of the leakage path through the interface the edge of the steel/bronze/polymeric counterpart is causing the pressure increase. The increased pressure at the edges is believed to play an important part in the leakage process. To visualize this effect carbon paper was put in between a pair of sealing rings and the imprint on the steel surface was studied. Figure 33 shows that most of the contact takes place where the edge of the smaller polymeric ring presses into the counterpart. This contact area increases with higher pressures.

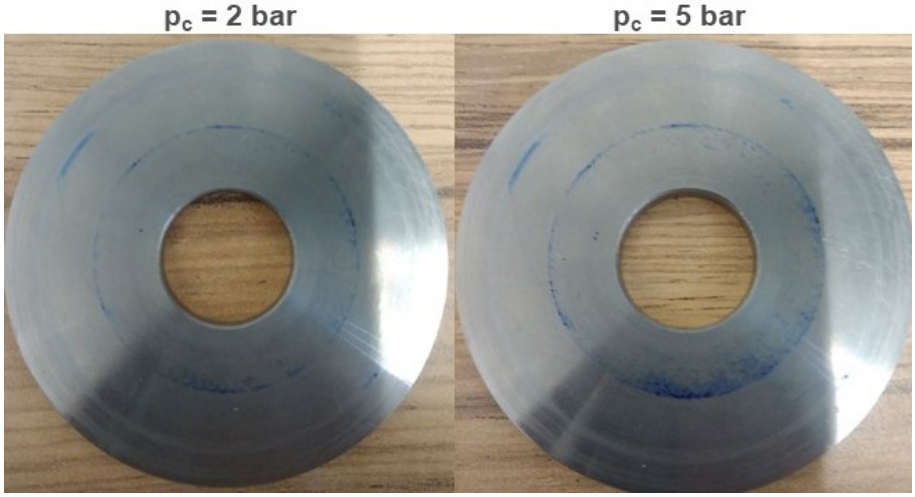

Figure 33: Visualization of the influence of the non constant pressure distribution of a flat punch.

It is believed that because of these circumstances a big part of the pressure drop

takes place at the beginning of the leakage path. Theoretically (cf. Chapter 2.4) the pressure profile that is built up by gas creeping into the interface should be independent from the nominal contact pressure and the surface structure. Therefore it should only depend on the nominal contact area. Kaufmann [3] developed an Abaqus calculation to model the gas pressure distribution in the arbitrarily shaped sealing interface. The gas pressure profile should theoretically only depend on the geometry of the interface. Its integral increases linearly with the applied pressure differential. Table 5 shows the nominal contact areas and the theoretical lifting force for different sealing lengths. The theoretical lifting force can be seen as the integral of the gas pressure distribution. In the experimental setup this force should be equal to the increase of normal force dF.

Table 5: Theoretical increase of the lifting force per bar differential pressure.

Sealing Length (mm)	**Nominal Contact Area** (mm^2)	**Increase of Lifting Force** (N/bar)
10	943	70
7.5	766	55
5	550	38

The leakage length can be varied by changing the inner diameter of the cover ring. As the dimensions of one ring and therefore the nominal area of the sealing interface change, the applied forces have to be changed to keep the nominal contact pressure the same. The contact pressure distribution (cf. Equation 9) also changes slightly, when the dimensions of the rings are changed. This effect cannot be prevented, but it is believed that its influence is minor. The recorded force dF at the same nominal contact pressures for different leakage lengths can be compared to the theoretical increase of the lifting force. Figure 34 shows an example of this comparison and it can be seen that higher nominal contact areas do not result in higher lifting forces. Multiple tests with different sealing pairs have been conducted and no clear correlation was found, which corroborates the theory that most of the pressure drop occurs at the edge at the beginning of the leakage path. Slight differences due to manufacturing fluctuations of the edge regions and measurement errors have a more significant impact than the actual sealing length.

The theoretical influence of the sealing length on the leakage can be found in Equation 21. When the nominal contact pressure stays the same the permeability K_ν and channel height h_c do not change. Therefore the leakage is only influenced by the ring dimensions and increases exponentially with decreasing sealing lengths. As the main pressure drop is taking place at the beginning of the leakage path, this theoretical dependency cannot be found in reality. Changes of the contact situation at the critical edge have a higher impact on the recorded leakage. The conducted tests did not show a clear tendency and shorter leakage lengths did not always result in higher leakages, as shown in Figure 35. A leakage length of 10 mm was chosen for the design of experiments as these are typical for the application.

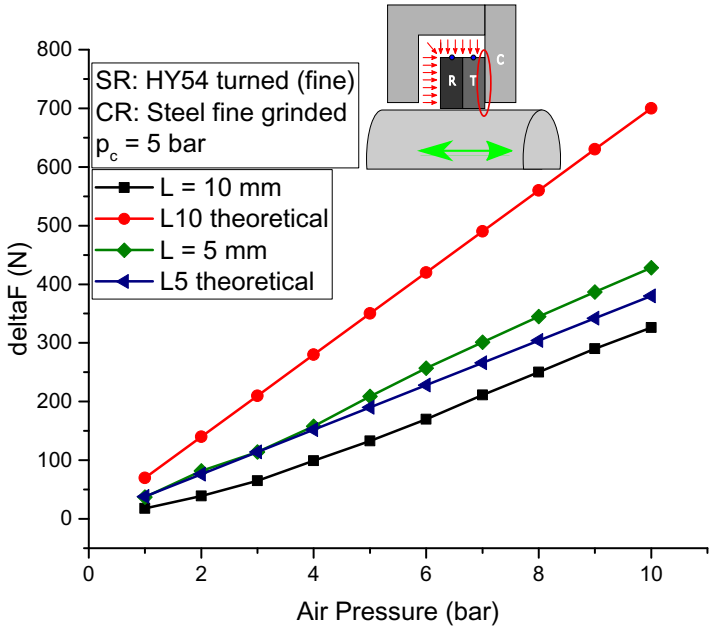

Figure 34: Comparison of the experimental with the theoretical lifting force.

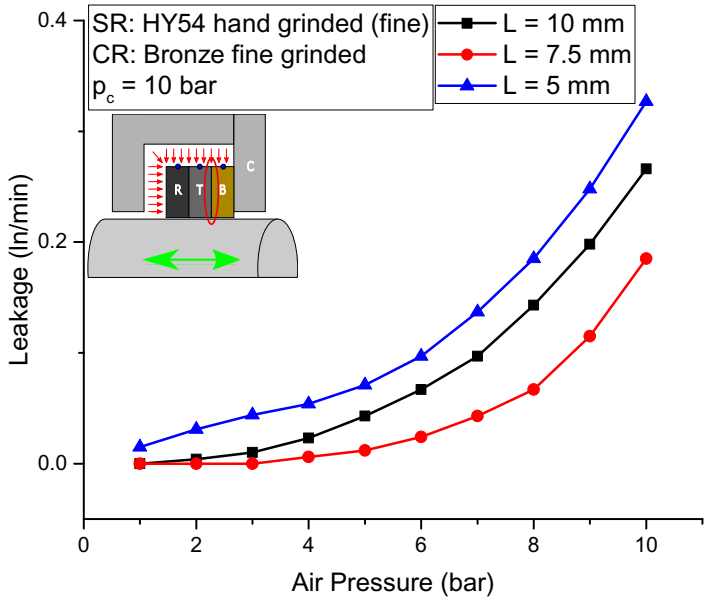

Figure 35: Influence of the sealing length on the leakage.

5.2 Analysis of Manufacturing Methods and Specimen

Before analysing the measurement method and the results, the obtained specimen characteristics are presented. The combination of material, manufacturing method and parameters define the flatness, the macroscopic shape and roughness of the surface, which are further discussed.

Figure 36 shows that turning metals leads to less deformed surfaces than turning polymers. The polymeric rings are turned out of semi-finished compression molded cylinders, called bushings. Residual stress due to the production and higher flexibility of the polymeric rings compared to metallic ones lead to higher deformation of the final ring. It needs to be stated, that the metallic rings are produced on a different machine using a different tool and slightly different parameters. The grinding operations for the various materials are entirely different processes. The lower flatness of the metallic surfaces is a combination of different material behavior and processes.

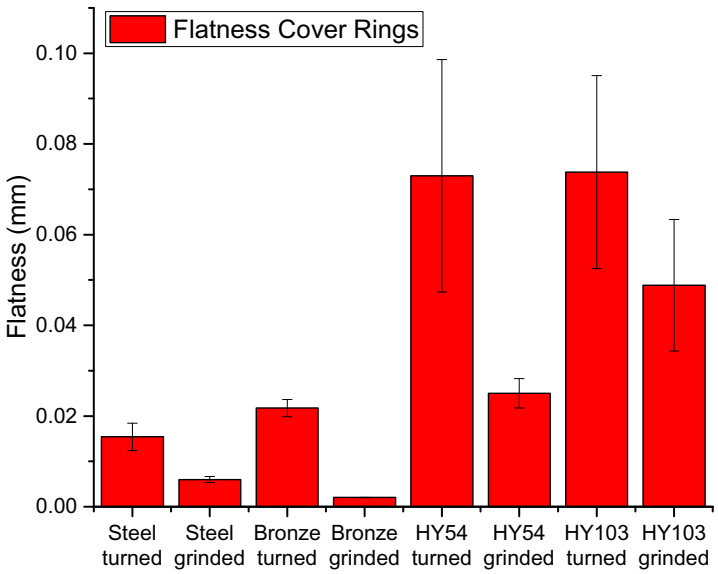

Figure 36: Flatness and standard deviation of cover rings manufactured with various methods.

Table 6 shows the obtained roughness values for the cover rings, manufactured with different machining methods. At least six rings were tested for each manufacturing method and the mean was calculated. The additional grinding process reduces the traditional roughness values R_a, R_v and R_{dq}. The change in skewness and kurtosis is rather small (cf. Figure 16), which is why their significance for predicting leakage is believed to be minor.

Table 6: Various roughness values of cover ring surfaces produced with different methods.

Material	Manufacturing Method	R_a (μm)	R_v (μm)	R_{sk} (-)	R_{ku} (-)	R_{dq} (μm)
Steel	turned (fine)	0.665	2.11	0.067	3.697	0.149
	grinded (fine)	0.275	1.194	-0.323	4.702	0.096
Bronze	turned (fine)	1.679	3.746	0.035	2.184	0.203
	grinded (fine)	0.390	1.781	-0.669	4.153	0.139
HY54 (PTFE)	turned (fine)	1.320	6.273	-0.778	4.459	0.209
	grinded (fine)	1.036	4.647	-0.739	4.046	0.151
HY103 (PEEK)	turned (fine)	0.755	2.569	-0.232	3.144	0.117
	grinded (fine)	0.631	2.474	-0.370	3.291	0.147

The polymeric stamp rings show a similar behavior as the polymeric cover rings. A full table of the flatness and roughness for the polymeric stamp rings can be found in the Appendix (Table 8 and 9). As an example, Figure 37 shows the flatness and the roughness R_a for all manufacturing methods for HY54. The turned rings are less flat than the hand grinded ones, but no significant difference in flatness can be found in between fine and coarse turned and between the fine and coarse grinded rings. On the contrary, the surface roughness decreases as expected when the feed rate is reduced and when finer sandpaper is used.

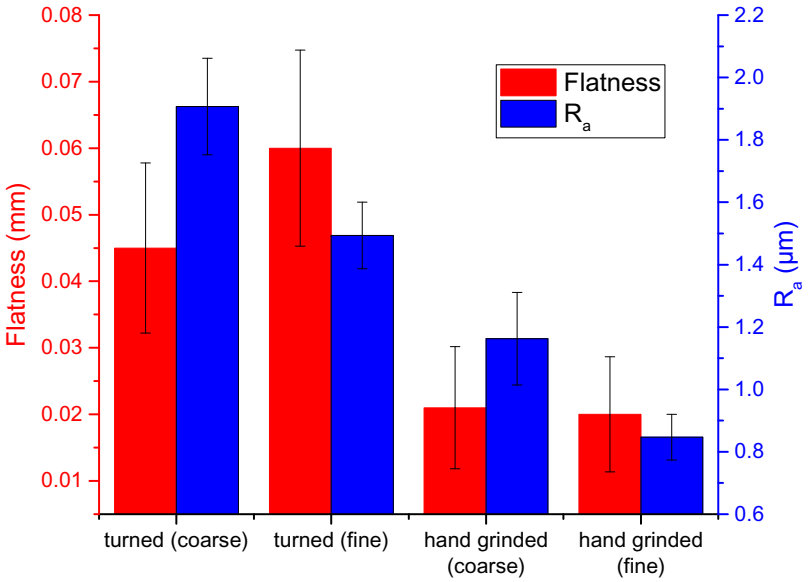

Figure 37: Flatness and roughness R_a of HY54 stamp rings manufactured with various methods.

All turned rings show a concave form. The magnitude of deformation for the different materials corresponds with the above discussed flatness. After grinding, the concave form remains, but the magnitude of the deformation can be reduced, which can be seen in Figure 38.

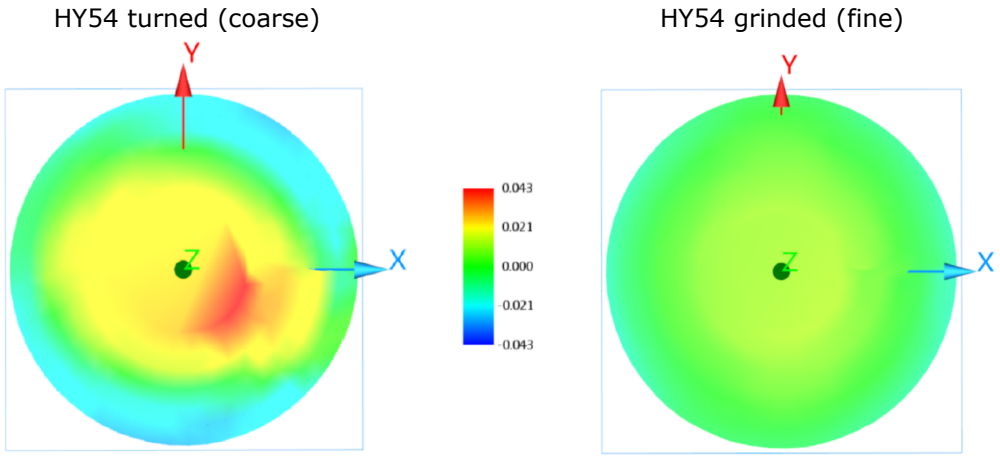

Figure 38: Deformation of a coarse turned and a fine grinded HY54 stamp ring.

5.3 Repeatability and Reproducibility

As viscoelasticity and irreversible deformation effect the repeatability study, the following procedure has been chosen to measure a valid repeatability:

- The chosen material pair is predeformed at a contact pressure of 15 bar to eliminate the influence of irreversible changes in the material.
- The material is stored for at least three days to allow time dependent deformations to reverse.
- The leakage is measured at a contact pressure of 3 bar for different gas pressures once per day. This allows most time dependent changes to reverse and the specimens are always approximately at the same initial state.

Figure 39 shows measurements performed with the same two rings as described above. The leakage decreases slightly over the course of a week. After two additional days, where no measurements were performed, the leakage is slightly higher again. The time needed for the viscoelastic deformations to reverse is greater than 24 hours. In general higher leakages result in absolute higher fluctuations. When the standard deviation of the scatter is put in relation to the mean leakage value for a specified gas pressure, a repeatability of about 5 % of the reading can be achieved. Therefore the significance of an effect can be estimated. An effect within a given material pair, for example a change in contact or gas pressure, must be at least 5 % to be seen as significant.

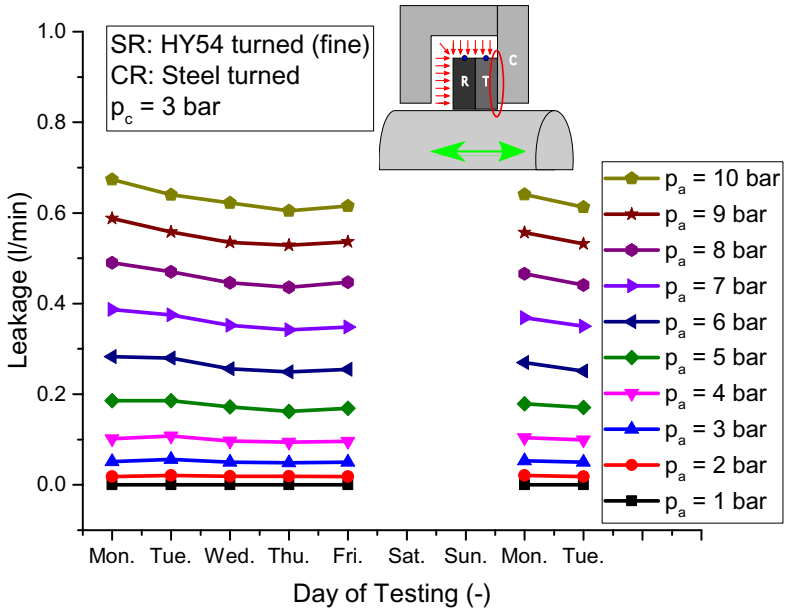

Figure 39: Variation of leakage rate measurements performed once per day.

Similar to the repeatability of the test rig, a reproducibility of the experiment can be evaluated. For this reproducibility test, six equally produced stamp rings were tested paired with one and the same cover ring. As the HY54 material grade shows the highest fluctuations in the machining process, it was chosen to be tested in this reproducibility study. The leakage tests were performed at a contact pressure of 5 bar and varied gas pressures. The recorded leakage of all six tests are shown in Figure 40. Similarly to the repeatability the absolute value of the standard deviation increases with higher leakages. Again the standard deviation can be divided by the mean leakage value for each gas pressure. It can be found that the reproducibility is about 25 % of the reading. In order to be seen as significant, changes in the leakage have to be greater than 25 % when different sealing rings are compared.

The values of the repeatability and reproducibility are good estimations and show the capabilities of the test rig and can be used to assess the validity of the results. Nonetheless it has to be pointed out that they were achieved by simplified repeatability and reproducibility studies. A full gauge repeatability and reproducibility study was not performed due to the material characteristics and limited test time.

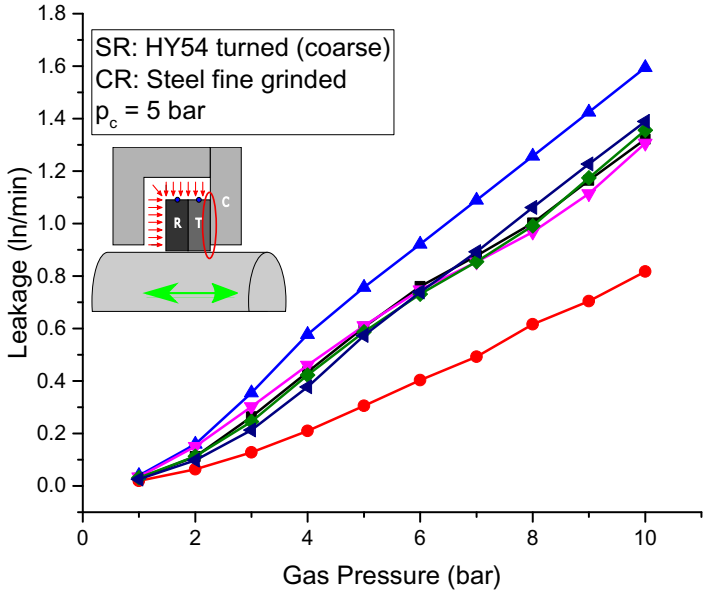

Figure 40: Leakage rate measurements for stamp rings (HY54). The six stamp rings are all turned with the same parameters and are paired with the same cover ring (steel).

5.4 Contact Pressure

The leakage highly depends on the contact situation between the two sealing surfaces and is therefore influenced by the contact pressure. In Chapter 5.1.3 values for the theoretical lifting force, which represents the integral of the gas pressure profile in the interface, were introduced. Using those, it can be shown that in the application the remaining mean contact pressure is theoretically about 30 % of the applied pressure differential. The gas creeping into the interface results in a pressure profile, which counteracts the contact pressure. For a gas pressure differential of 10 bar ($= 1$ N/mm^2) the integral of this pressure profile is 0.7 N/mm^2. A mean pressure of about 30 % of the applied pressure differential remains. The test rig increases its holding force when the gas pressure increases. Therefore the parts of the tests, where the contact pressure equals about 30 % of the gas pressure are of interest. This is also the region, where the discussed leakage models are not valid any more, as the gas pressure exceeds the contact pressure.

All discussed theories predict an exponential decrease of leakage with an increase of contact pressure. The introduced theories are only for purely elastic or elastic-plastic contact, while the examined materials show viscoelastic and plastic behavior. Still the results are compared qualitatively to theoretical models. The conducted experiments also show an exponential decrease of leakage with an increasing contact pressure. Figure 41 shows such a typical decrease of leakage for a HY54 and steel sealing ring pair. Examples for all other material pairs can be found in the

Appendix (Figures 52, 53, 54, 55). The growth rate is dependent on surface and material properties, such as flatness, roughness, (visco)elastic and plastic properties. The influence of flatness and roughness (Chapter 5.6) and of the materials (Chapter 5.7) are later discussed separately.

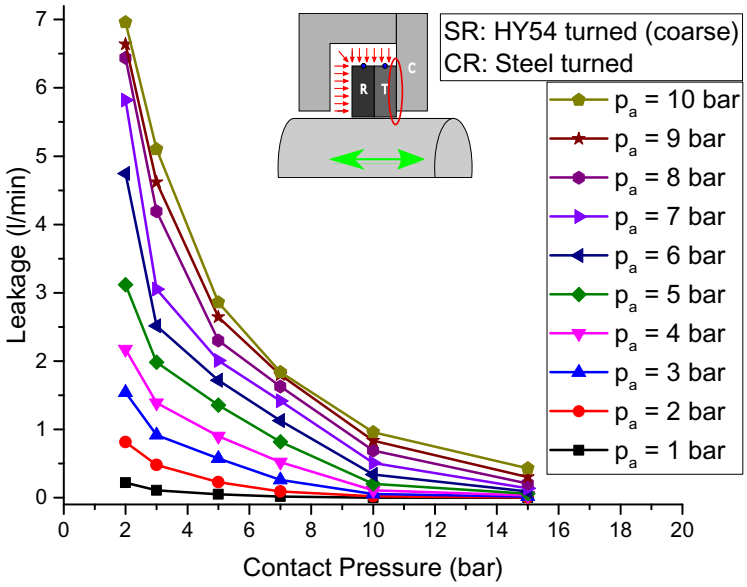

Figure 41: Influence of the contact pressure on the leakage for different applied gas pressures for a combination of HY54 and steel.

For the combination of two softer rings (HY54), this theoretical dependency can only be found for contact pressures greater than the applied gas pressures. A combination of macroscopic deformations due to the contact pressure and the gas pressure lead to the behavior shown in Figure 42. It is believed that for small apparent contact pressures the edge of the smaller ring is the main factor for the small leakage. The concave shape of the ring results in a small contact area and therefore higher local pressures. Once the apparent contact pressure is further increased, the ring is further deformed, resulting in a larger real contact area. The high pressure at the edge decreases, allowing the gas to creep in easier.

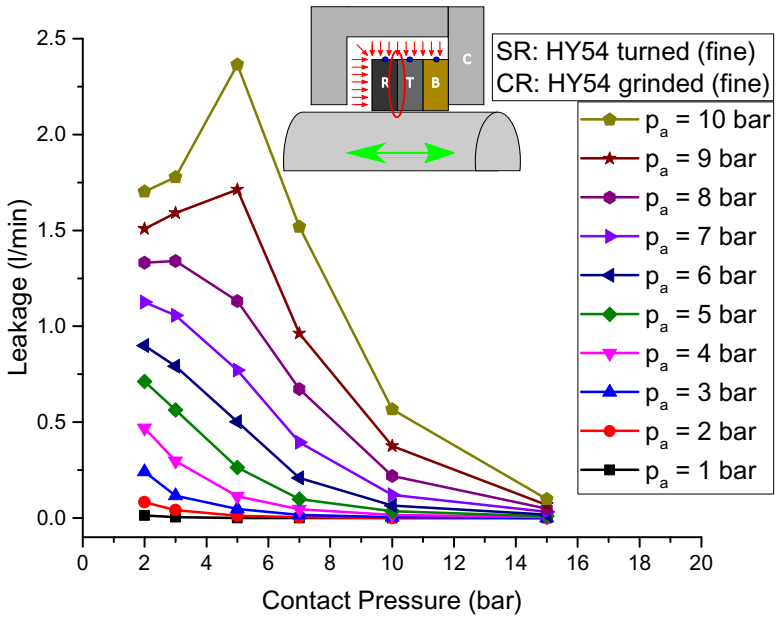

Figure 42: Influence of the contact pressure on the leakage for different applied gas pressures for a combination of HY54 and HY54.

5.5 Gas Pressure

The second testing parameter that influences the leakage is the applied gas pressure. Most theoretical models are only valid if the contact pressure exceeds the gas pressure. In this case the influence of the gas pressure on the contact situation can be neglected and a linear increase of the leakage with increasing pressure differential is expected. Only one of the discussed theoretical models (cf. Figure 22) is able to include the gas pressure influence on the interface between the sealing rings. The leakage increases more rapidly once the gas pressure reaches about 60% of the contact pressure, which is confirmed by the conducted tests. Figure 43 gives an example of the dependence of leakage on the gas pressure for a combination of HY103 and bronze. Other examples can be found in the Appendix (Figures 56, 57, 58, 59). As discussed in the section before, for a combination of two soft rings (HY54) this dependency is only true for contact pressures greater than the applied gas pressures. An example for this can also be found in the Appendix (Figure 60).

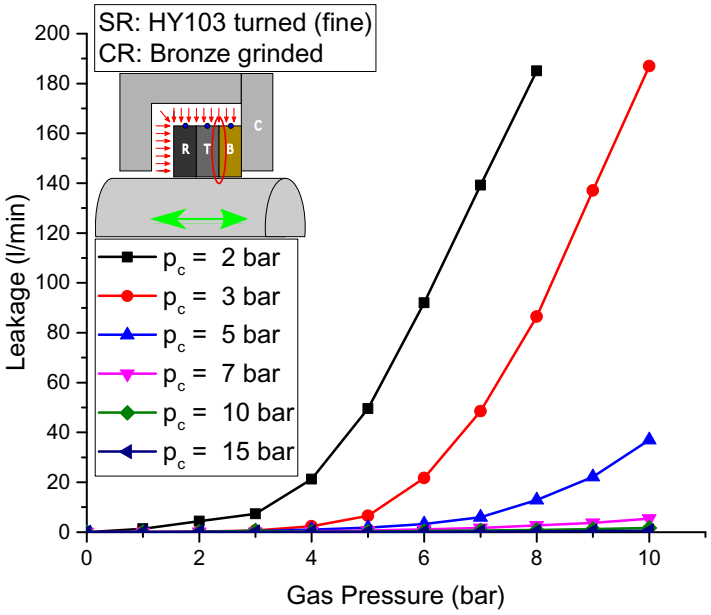

Figure 43: Influence of the gas pressure on the leakage for different contact pressures for a combination of HY103 and bronze.

5.6 Surface Quality Influence: Manufacturing Method, Flatness and Roughness

The leakage through a sealing ring pair is dependent on the surface quality. Changes in leakage can occur due to a difference in flatness and roughness. Table 8 and 9 show that changing the feed rate in the face turning operation has little effect on the flatness of the final part. On the contrary, the roughness can be manipulated. Similarly, the flatness does not significantly change, when using a finer grit in the hand grinding process, while the roughness is influenced. Nonetheless the measured leakage is always a combination of these two and other factors. It cannot be stated with certainty, if changes in leakage are due to a difference in flatness or roughness. As the two polymers show different behaviors, the manufacturing influence is further discussed separately for each material.

5.6.1 HY54

Because HY54 is a relatively soft material, the influence of the flatness on the leakage can be neglected. Even at small nominal contact pressures soft polymeric materials can easily be deformed. This can be seen in Figure 33. Even at small pressures all of the edge of the smaller ring imprints on the cover ring. Additionally, the fine turned HY54 rings leak less than the coarse turned ones, although their surface is less flat. Similarly, the rings grinded with finer sandpaper result in less leakage while having similar flatness. The better performance is due to the decreased roughness, which has a more significant impact on the leakage than the flatness.

For the polymeric rings not only the manufacturing methods, but also the manufacturing parameters (see Chapter 4.4) were changed. The feed rate was changed in the turning process. An increase of the feed rate results in a rougher surface, which is confirmed by Fetecau [35]. The hand grinding process was performed with two different grit sizes of sandpaper. The theory predicts, that coarser grits result in rougher surfaces. Figure 44 shows a sealing ring pair, where the HY54 ring was varied, while the bronze ring was kept the same. The grinded surfaces perform better than the turned ones. Additionally, it can be seen that higher feed rates in the turning and coarser grit sizes in the grinding operation have a negative impact on the sealing function. The same trends can be found for steel paired with HY54, see Figure 61 in the Appendix.

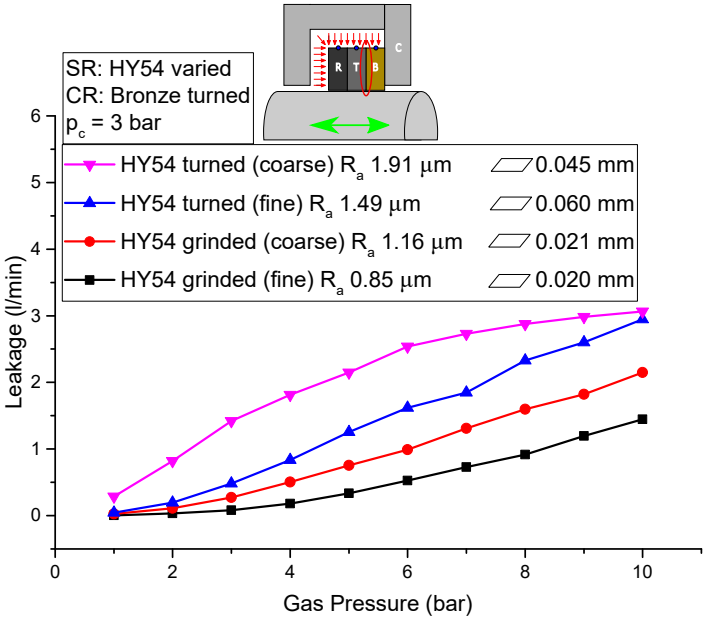

Figure 44: Influence of the manufacturing method of HY54 rings on the leakage for a contact pressure of 3 bar and a combination with bronze.

The different manufacturing methods result in a difference in surface roughness. Figure 45 shows the dependency of the leakage on the roughness R_{dq} and Figure 46 the dependency on the roughness R_{a}. Other roughness values that can be used to describe this dependency are the maximum depth of valleys R_{v} and the root mean square roughness R_{q}. Examples of the leakage dependency on these two roughness values can be seen in Figure 62 and 63, which can be found in the Appendix. The manufactured surfaces show higher kurtosis R_{ku} with lower arithmetic roughness R_{a}. Kotwal and Bhushan [23] found that theoretically, for surface profiles with the same roughness R_{a}, lower kurtosis values lead to higher real contact areas and therefore less leakage. The influence of the decrease of the arithmetic roughness has a more significant effect than the increase in kurtosis. Therefore the increase in kurtosis

does not lead to higher leakages. The theoretical optimum of the skewness R_{sk} is between 0 and 1 [23]. As all manufactured surfaces lie in this optimum area, the influence of changes is minor and therefore cannot be detected. As long as skewness and kurtosis are in the obtained range, it is sufficient to only control and minimize the more common roughness parameters R_a, R_v, R_q and R_{dq}, where the root mean square slope of the profile R_{dq} is the only parameter that theoretically can be directly linked to the real contact area.

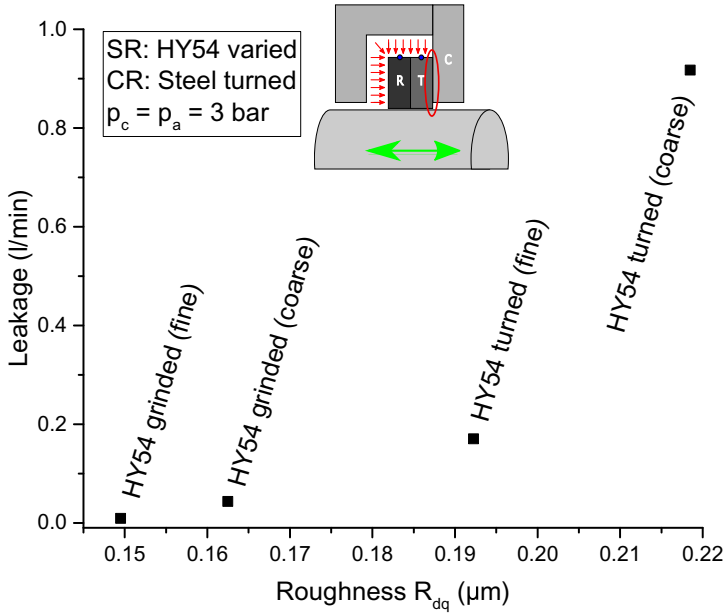

Figure 45: Influence of the roughness R_{dq} of HY54 rings on the leakage for a contact and gas pressure of 3 bar and a combination with steel.

Again for a sealing pair of two polymeric rings, these dependencies are only valid if the contact pressures are higher than the gas pressure. For a contact pressure of 15 bar the theoretical dependencies are observed, which can be seen in the Appendix (Figure 64). Once the gas pressure exceeds the contact pressure macroscopic deformation can take place and the detailed deformation processes are not known any more. Figure 47 shows, that for gas pressures smaller than the contact pressure, the usual dependency can be found. Once gas pressures are increased further this changes and leakage is mainly influenced by those macroscopic deformations.

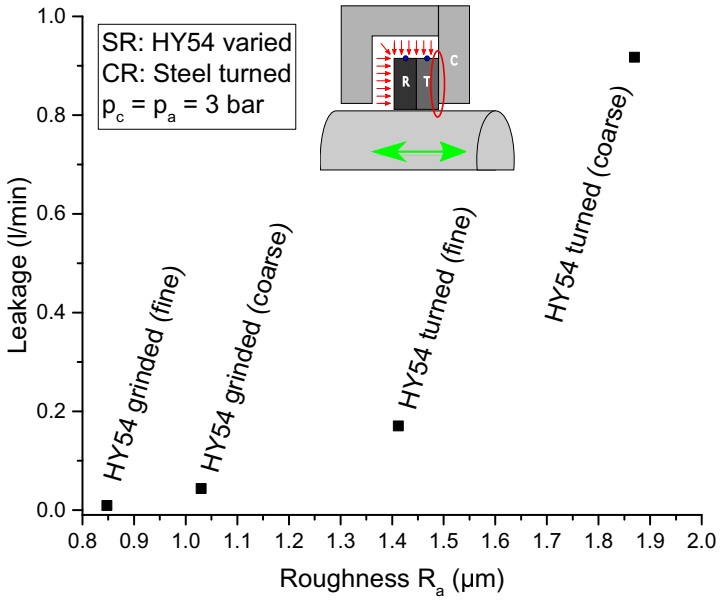

Figure 46: Influence of the roughness R_a of HY54 rings on the leakage for a contact and gas pressure of 3 bar and a combination with steel.

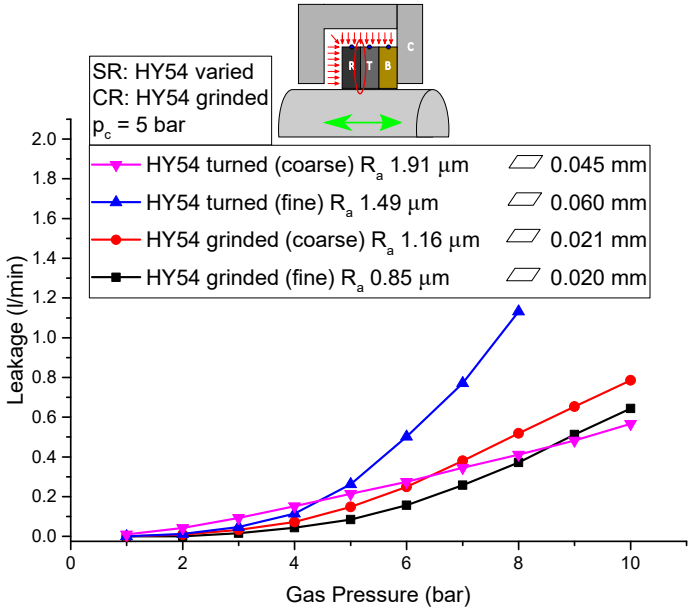

Figure 47: Influence of the manufacturing method of HY54 rings on the leakage for a contact pressure of 5 bar and a combination with HY54.

5.6.2 HY103

In general all tests performed with the more rigid HY103 material lead to higher leakage. When only the roughness influence is considered, materials with higher moduli lead to higher leakage, as the roughness asperities are not as easily deformed. Nonetheless, the recorded leakage increase should be in the same order of magnitude. Especially at low contact pressures very high leakage is detected. Therefore the increase is not solely based on a change in the microscopic behavior. Although the flatness of the HY103 rings is approximately the same as for the HY54, in this case the flatness influence is not neglectable. At low contact pressures the stiffer HY103 rings are not deformed enough, which results in gaps that exceed the order of magnitude of the roughness and gas can easily creep into the interface. This is particularly noticeable for the less flat turned rings, while the grinded rings behave similar to the HY54 rings. Figure 48 shows the visulization of the contact between a coarse turned HY103 and a turned steel plate for several contact pressures.

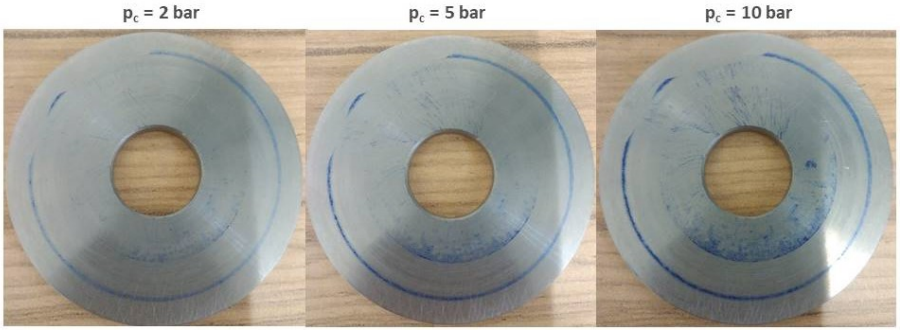

Figure 48: Visualization of the contact of a coarse turned HY103 ring and a turned steel ring.

The influence of the manufacturing method on flatness and leakage can be seen for HY103 in combination with bronze in Figure 49 and in combination with steel in the Appendix (Figure 65).

5.6.3 Bronze and Steel

For the cover ring materials bronze and steel the manufacturing methods have been changed as well. When solely concentrating on the influence of the manufacturing methods, it can be found that turned surfaces perform worse than grinded surfaces. This is due to the fact that grinding operations usually result in flatter and less rough surfaces. Exemplary, Figure 50 shows a comparison between two differently manufactured bronze cover rings paired with a fine grinded PTFE (HY54) stamp ring. This dependency can be found for bronze/steel rings paired with polymeric rings. An example for a steel ring paired with a HY103 ring can be found in Figure 66 in the Appendix.

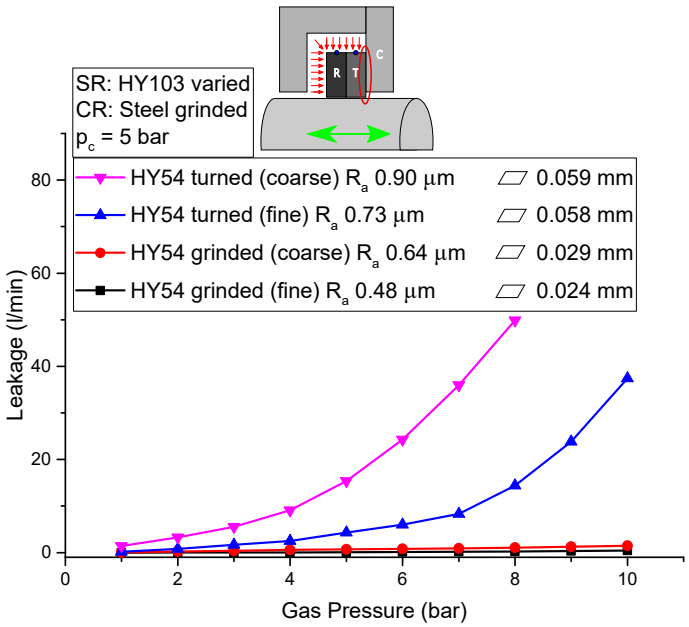

Figure 49: Influence of the manufacturing method of HY103 rings on the leakage for a contact pressure of 5 bar and a combination with steel.

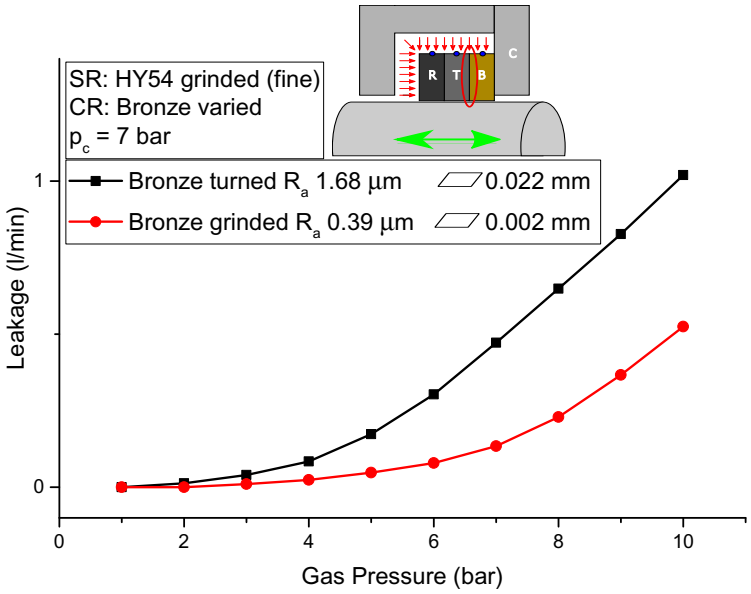

Figure 50: Influence of the manufacturing method of the bronze ring on the leakage for a contact pressure of 7 bar and a combination with HY54.

5.7 Comparison of Materials

Other than the testing and surface parameters, a comparison of the used materials is of interest and concludes the investigations. In a packing ring group different material combinations contribute to the total leakage. For this comparison, typical ring groups with and without a backup ring are considered. This comparison is focusing on the manufacturing procedures currently used at HOERBIGER Wien GmbH. Sealing ring surfaces are hand grinded with a fine grid size, bronze backup rings are fine grinded and the cup faces are surface grinded.

First, the combination of a radial ring, a tangential ring and the cup is considered. Figure 51a shows the leakage interfaces i and iv. As the contact pressures in the application equal about 30 % of the gas pressure differential (cf. Chapter 2.4), a contact pressure p_c of 3 bar and a gas pressure p_a of 10 bar is chosen for this estimation. In the case of the soft PTFE based material (HY54), the main factor influencing the leakage is the roughness of the materials in contact. The fine grinded HY103 rings are flat enough, so that the influence of the flatness of the rings is minor and the leakage is mainly influenced by the roughness as well. Table 7 lists the contribution from each sealing interface to the total leakage. Leakage between two polymeric rings is higher than the one through a polymeric ring and a metal ring. This can be explained by the finer surface of the metal rings, while the general deformability of the asperities is determined by the softer material, which stays the same. Although the fine hand grinding of the harder HY103 material results in a less rough surface than for an equally manufactured HY54 ring, the leakage is higher. Due to the higher modulus and hardness of the material, the asperities are not as easily deformed resulting in larger leakage channels. In general it can be said, that the leakage in both cases is minor.

Figure 51b shows the leakage interfaces for a packing ring group with a backup ring. A comparison of the contributions from each interface to the total leakage can be found in Table 7. For a combination of bronze and steel both rings are not easily deformed, therefore this combinations leaks heavily for small contact pressures. At a contact pressure p_c of 3 bar and a gas pressure p_a of 10 bar the leakage is more than 200 l/min. Although the metallic rings are very flat, this low contact pressure is not able to close the gaps. In general, especially for low contact pressures the flatness plays a dominant role. Therefore, a contact and a gas pressure of 10 bar were chosen to compare the contribution of the different material pairs to the total leakage. All of the observations made at the packing ring group without a backup ring are true as well. Additionally, it can be seen, that most leakage occurs through pairs of metallic rings. At low contact pressures this is due to the flatness, which cannot be overcome by the pressure. At higher pressures the dominant leakage of the metal pair is less, but still evident. Although these rings are less rough than the polymeric rings, the asperities are not as easily deformed, resulting in higher leakage.

Typical leakages through packing ring groups in compressors exceed the leakages found in this study by an order of magnitude. Therefore the main part of the leakage does not occur in between the faces of the rings, but occur due to machining

imperfections.

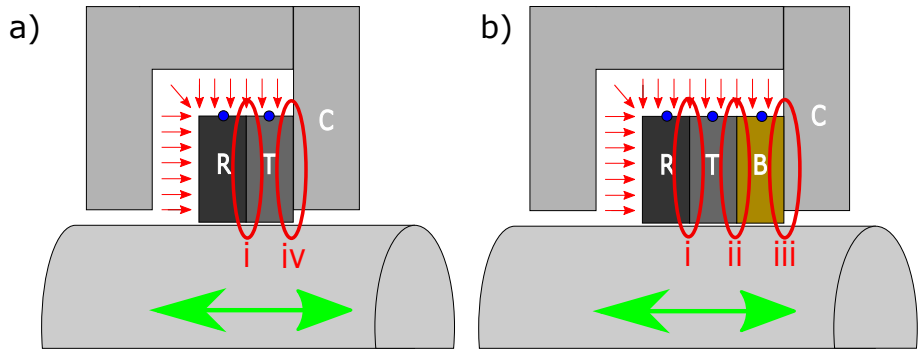

Figure 51: Definition of the sealing surfaces for a packing ring group with (a) and without (b) a backup ring. The contributions for different material pairs can be found in Table 7.

Table 7: Contribution of different sealing surface to the total leakage for different packing ring groups and different contact and gas pressures. The sealing interfaces i, ii, iii and iv are defined in Figure 51.

Ring Group	**R & T Material**	$\mathbf{p_c}$ (bar)	$\mathbf{p_a}$ (bar)	**Leakage Through Interface** i (l/min)	ii (l/min)	iii (l/min)	iv (l/min)	**Total Leakage** (l/min)
RTC	HY54	3	10	0.688			0.475	1.163
	HY103	3	10	1.529			0.624	2.153
RTBC	HY54	10	10	0.262	0.269	1.349		1.880
	HY103	10	10	0.541	0.157	1.349		2.047
	HY54/HY103	3	10	< 2	< 2	> 200		> 200

6 Resume

The aim of this thesis was to examine the influence of material, manufacturing and test parameters on the leakage of static sealing surfaces of sealing elements, which are used in compressor packings. Therefore a newly designed test rig was manufactured, which allows to independently apply the contact pressure between two sealing rings and the gas pressure. Influencing disruptive factors in the experimental setup were identified and reduced as far as possible.

Sealing rings were manufactured by turning with different machining parameters to investigate the influence of the manufacturing parameters. Additionally, the ring surfaces were treated by different grinding processes for each material and for polymeric rings the grit size of the sandpaper was varied. The grinding of ring surfaces is typical in the production of such seals. This resulted in different surfaces with different roughness and flatness. All materials were tested as combinations, as usually found in a compressor packing.

Before any testing was performed, disruptive factors that might influence the results were identified and studied:

- The typical viscoelasticity of polymers leads to time dependent effects.
- Deformations prior to testing have to be taken into account. Asperities, which are plastically deformed, influence the contact situation between the two bodies.
- The distribution of the contact pressure is not uniform. Higher pressures can be detected at the edges of the sealing elements, even for nominally flat surfaces. Additionally, the contact pressure distribution is influenced by prior deformations of the surface due to the manufacturing process.

The theoretical prediction, that higher contact pressures result in a logarithmic decrease of leakage, were qualitatively confirmed. The more recent and more complicated theories, which predict this logarithmic dependency, cannot be used for a quantitative comparison, as additional fractal input parameters would be necessary. Easier leakage models can only be used for purely elastic deformations of metal asperities and therefore give no valid quantitative or qualitative comparison. As for the conducted experiments the applied gas pressure is in the order of and partially exceeds the contact pressure, its influence on the contact situation cannot be neglected. Therefore the theoretical linear increase can only be seen for high contact pressures and low gas pressures. Once the gas pressure equals the contact pressure, the leakage increases more rapidly when the gas pressure is further increased.

The manufacturing method and parameters determine the obtained surface quality. Macroscopic surface deformations can be compensated even at low contact pressures, as long as the materials are soft. Therefore the influence of the flatness of the rings is minor and the leakage is mainly determined by the roughness. Smoother

surfaces lead to smaller leakage paths and thus reduced leakage.

More rigid materials cannot be deformed as easily. Especially at low contact pressures the leakage is determined by the flatness. The size of the gaps between the two surfaces is about the size of the flatness, which results in high leakage. Contact pressures need to be high to compensate non flat surfaces. If the deformation of the plates is compensated, the leakage is mainly determined by the roughness again. In conclusion, it can be said that flatter and smoother surfaces and softer materials lead to less leakage.

This is also noticeable when studying the contribution to the total leakage for different material pairs. As long as one of the rings in contact is deformed easily, the flatness plays a minor role. Most leakage occurs through metallic sealing pairs as both surfaces are not easily deformed. Non flat surfaces are not compensated by low contact pressures leading to very high leakage. Even for high contact pressures, where the rings are macroscopically deformed, the combination of metallic rings show the highest leakage, as the asperities are not as easily deformed.

This thesis allows to estimate leakage through static sealing areas in a ring group not only quantitatively, but also quantitatively. The test rig allows to extend the already existing models, so that the viscoelastic behaviour of polymers can be considered. Conclusions on the leakage in compressors can be drawn. Most leakage occurs in the joint areas due to manufacturing imperfections.

Acronyms and List of Symbols

Acronyms

B	backup ring
BCD	balanced cap design
C	face of the cup
CR	cover ring
PAI	polyamide imide
PEEK	polyether ether ketone
PI	polyimide
PTFE	polytetra fluoroethylene
R	radial cut ring
RMS	root-mean-square
SR	stamp ring
T	tangential cut ring

List of Symbols

α	leakage channel correction factor
A_0	nominal contact area
A_ζ	area as a function of the magnification
A_r	real area of contact
b	half of the side length of a flat planar punch
$C(q)$	power spectral density
ΔP	pressure drop across a seal
$d_{\mathrm{o,CR}}$, $d_{\mathrm{i,CR}}$	outer, inner diameter of the contact ring
$d_{\mathrm{o,SR}}$, $d_{\mathrm{i,SR}}$	outer, inner diameter of the stamp ring
$\mathrm{d}F$	compensation force to keep the traverse at its position
E^*	effective modulus
$E_{1,2}$	modulus of the two bodies in contact
$E(t)$	time dependent modulus of viscoelastic materials
ζ	magnification
ζ_c	critical magnification
F_C	applied contact force
F_N	applied normal force
η	dynamic fluid viscosity
H	surface indentation hardness
h	mean separation of two surfaces in contact
h_c	vertical height of the percolation channel
$\Theta(x)$	slope of the profile at the position x

K_ν	permeability of the interface
λ	macroscopic length scale
λ_c	lateral size of the most narrow constriction
L	contact length
L_x, L_y	side lengths of a rectangular seal
$\nu_{1,2}$	Poisson's ratio of the two bodies in contact
N	number of identical squares within a rectangular seal
n	density of asperity summits per unit area
P	force applied on a flat punch
p_0	gas pressure after a ring group or a sealing ring
p_a	gas pressure before a packing ring group or a sealing ring
p_c	apparent contact pressure
$p_\mathrm{c,flat}$	theoretical contact pressure assuming microscopically perfectly at surfaces
$p_\mathrm{c,rough}$	theoretical contact pressure reduced by the gas pressure in the dynamic sealing surface w
p_crk	crank side gas pressure
p_cyl	cylinder side gas pressure
p_g	integral of the gas pressure profile in a sealing interface
$p_\mathrm{g}(r)$	gas pressure profile in a sealing interface as a function of the radius
p_m	mean pressure of a flat punch
$P_{\sigma,\zeta}$	local stress distribution as a function of the magnification
$P(t)$	cumulative probability distribution function
$p(y)$	profile probability density function
Q	Leakage

q	wave vector
R_{a}	arithmetic average height of the roughness profile
R_{dq}	root means square slope of the roughness profile
r_{i}, r_0	inner, outer radius of the circular sealing interface
R_{ku}	kurtosis of the roughness profile
R_{p}	radius of the spherical bumps of a theoretical surface
R_{q}	root mean square roughness of the roughness profile
R_{sk}	skewness of the roughness profile
R_{v}	maximum depth of valleys of the roughness profile
σ_{p}	standard deviation of the height distribution of a roughness profile
σ_{y}	yield strength
S_{q}	root mean square roughness of the roughness profile
t	given distance to the mean line of a roughness profile
$u_1(\zeta_c)$	separation of two surfaces at the critical magnification
Φ	plasticity index
$y(x)$	measured line profile of a surface

References

[1] Heinz P. Bloch and John J. Hoefner. *Reciprocating compressors: Operation & maintenance*. Gulf Pub. Co, Houston, Tex., 1996.

[2] Tony Giampaolo. *Compressor handbook: Principles and practice*. Fairmont Press and Distributed by Taylor & Francis, Lilburn, GA and Boca Raton, FL, 2010.

[3] Andreas Kaufmann. *Wear of dry-running piston rod sealing rings: modelling and experiments*. PhD thesis, Montanuniversität Leoben, Leoben, 2018.

[4] Paul C. Hanlon, editor. *Compressor handbook*. McGraw-Hill, New York, 2001.

[5] Chris Radcliffe. Sealing material developments for reciprocating gas compressors. *Sealing Technology*, 2005(11):7–11, 2005.

[6] Norbert Feistel. Performance improvement of dry-running sealing systems by optimization of wear compensation. *Conference of the European Forum for Reciprocating*, pages 239–247, 2014.

[7] E. Cummings. Mechanical packing design and theory of operation. 2011.

[8] Norbert Feistel. *Beitrag zum Betriebsverhalten trocken laufender Dichtsysteme zur Abdichtung der Arbeitsräume von Kreuzkopfkompressoren*. Dissertation, Universität Erlangen-Nürnberg, Erlangen-Nürnberg, 2001.

[9] Bharat Bhushan. *Introduction to tribology*. Tribology in Practice Series. John Wiley & Sons, 2. edition.

[10] Qiang Zhang, Xiaoqian Chen, Yiyong Huang, and Xiang Zhang. An experimental study of the leakage mechanism in static seals. *Applied Sciences*, 8(8):1404, 2018.

[11] Bharat Bhushan, editor. *Modern tribology handbook*. Mechanics and materials science series. CRC Press, Boca Raton, Fla., 2001.

[12] E. S. Gadelmawla, M. M. Koura, T.M.A. Maksoud, I. M. Elewa, and H. H. Soliman. Roughness parameters. *Journal of Materials Processing Technology*, 123(1):133–145, 2002.

[13] Jiajin Qu. Non-ra roughness parameters of shaft surfaces for radial lip seal applications. In *SAE Technical Paper Series*, SAE Technical Paper Series. SAE International400 Commonwealth Drive, Warrendale, PA, United States, 1995.

[14] Tevis D. B. Jacobs, Till Junge, and Lars Pastewka. Quantitative characterization of surface topography using spectral analysis. *Surface Topography: Metrology and Properties*, 5(1):013001, 2017.

[15] Han Haitjema. Flatness. In Luc Laperrière and Gunther Reinhart, editors, *CIRP Encyclopedia of Production Engineering*, volume 29, pages 1–5. Springer, Berlin and Heidelberg, 2014.

[16] Bianca Maria Colosimo, Ester Gutierrez Moya, Giovanni Moroni, and Stefano Petrò. Statistical sampling strategies for geometric tolerance inspection by cmm. *Economic Quality Control*, 23(1):28, 2008.

[17] David Roylance. Introduction to fracture mechanics, 2001.

[18] Valentin Leonidovič Popov. *Kontaktmechanik und Reibung: Ein Lehr- und Anwendungsbuch von der Nanotribologie bis zur numerischen Simulation*. Springer Berlin Heidelberg, Berlin, Heidelberg, 2009.

[19] B.N.J. Persson. Contact mechanics for randomly rough surfaces. *Surface Science Reports*, 61(4):201–227, 2006.

[20] Hamid Ghaednia, Xianzhang Wang, Swarna Saha, Yang Xu, Aman Sharma, and Robert L. Jackson. A review of elastic–plastic contact mechanics. *Applied Mechanics Reviews*, 69(6):060804, 2017.

[21] Chetan A. Kotwal and Bharat Bhushan. Contact analysis of non-gaussian surfaces for minimum static and kinetic friction and wear. *Tribology Transactions*, 39(4):890–898, 1996.

[22] N. H. Cook and B. Bhushan. Sliding surface interface temperatures. *Journal of Lubrication Technology*, 95(1):59, 1973.

[23] D. Tabor. The hardness of solids. *Review of Physics in Technology*, 1(3):145.

[24] Paul Bauer. Inverstigation of leakage and sealing parameters, 1965.

[25] F. P. Bowden and D. Tabor. *The friction and lubrication of solids*. Oxford classic texts in the physical sciences. Oxford University Press, Oxford, 2001.

[26] B. N. Persson. Elastoplastic contact between randomly rough surfaces. *Physical review letters*, 87(11):116101, 2001.

[27] B. N. J. Persson. Theory of rubber friction and contact mechanics. *The Journal of Chemical Physics*, 115(8):3840–3861, 2001.

[28] Boris Lorenz. *Contact mechanics and friction of elastic solids on hard and rough substrates: Aachen, Techn. Hochsch., Diss., 2012*, volume 37 of *Schriften des Forschungszentrums Jülich / Reihe Schlüsseltechnologien*. Hochschulbibliothek Rheinisch-Westfälische Technischen Hochschule Aachen, Aachen, 2012.

[29] B. N. J. Persson, O. Albohr, C. Creton, and V. Peveri. Contact area between a viscoelastic solid and a hard, randomly rough, substrate. *The Journal of Chemical Physics*, 120(18):8779–8793, 2004.

[30] B. N. J. Persson and C. Yang. Theory of the leak-rate of seals. *Journal of Physics: Condensed Matter*, 20(31):315011, 2008.

[31] Qiang Zhang, Xiaoqian Chen, Yiyong Huang, and Yong Chen. Fractal modeling of fluidic leakage through metal sealing surfaces. *AIP Advances*, 8(4):045310, 2018.

[32] B. N. J. Persson, O. Albohr, U. Tartaglino, A. I. Volokitin, and E. Tosatti. On the nature of surface roughness with application to contact mechanics, sealing, rubber friction and adhesion. *Journal of Physics: Condensed Matter*, 17(1):R1–R62, 2005.

[33] B. N. J. Persson. Fluid dynamics at the interface between contacting elastic solids with randomly rough surfaces. *Journal of Physics: Condensed Matter*, 22(26):265004, 2010.

[34] R. K. Flitney and Melvin W. Brown. *Seals and sealing handbook*. Elsevier, Oxford, 5th ed. edition, 2007.

[35] Catalin Fetecau and Felicia Stan. Study of cutting force and surface roughness in the turning of polytetrafluoroethylene composites with a polycrystalline diamond tool. *Measurement*, 45(6):1367–1379, 2012.

[36] Gottfried Ehrenstein. *Polymer-Werkstoffe: Struktur ; Eigenschaften ; Anwendung*. Carl Hanser Fachbuchverlag, s.l., 3. aufl. edition, 2011.

[37] J. S. McFarlane, D. Tabor. Adhesion of solids and the effect of surface films. *Proceedings of the Royal Society of London. Series A. Mathematical and Physical Sciences*, 202(1069):224–243, 1950.

List of Figures

List of Tables

Appendix

Table 8: Roughness values of the HY54 stamp ring surfaces produced with different methods.

Manufacturing Method	**Flatness** (mm)	$\mathbf{R_a}$ (μm)	$\mathbf{R_v}$ (μm)	$\mathbf{R_{sk}}$ (-)	$\mathbf{R_{ku}}$ (-)	$\mathbf{R_{dq}}$ (μm)
Turned (coarse)	0.045	1.907	7.732	-0.641	3.745	0.206
Turned (fine)	0.060	1.494	7.142	-0.916	4.554	0.193
Grinded (fine)	0.021	1.163	5.722	-0.806	4.510	0.179
Grinded (coarse)	0.020	0.847	4.639	-1.053	5.323	0.150

Table 9: Roughness values of the HY103 stamp ring surfaces produced with different methods.

Manufacturing Method	**Flatness** (mm)	$\mathbf{R_a}$ (μm)	$\mathbf{R_v}$ (μm)	$\mathbf{R_{sk}}$ (-)	$\mathbf{R_{ku}}$ (-)	$\mathbf{R_{dq}}$ (μm)
Turned (coarse)	0.059	0.895	3.163	-0.333	3.090	0.137
Turned (fine)	0.058	0.731	2.406	-0.175	2.876	0.123
Grinded (fine)	0.028	0.648	2.309	0.037	3.393	0.175
Grinded (coarse)	0.024	0.478	1.823	-0.252	3.350	0.139

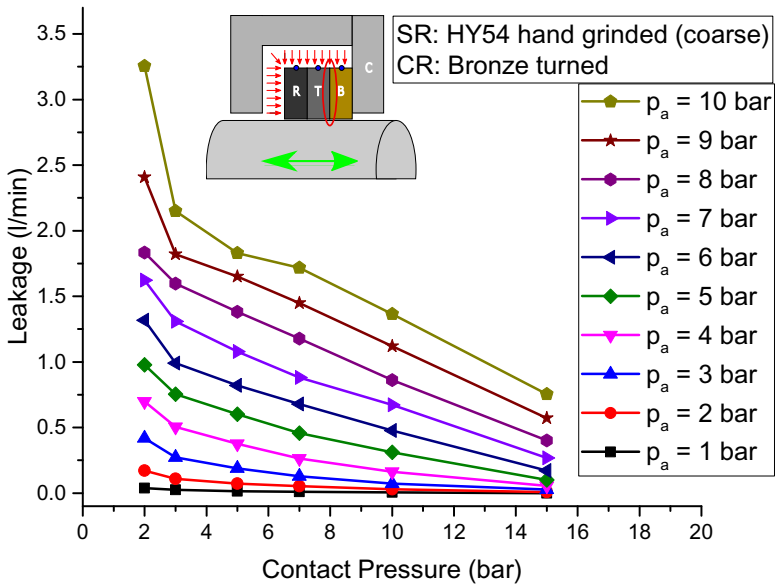

Figure 52: Influence of the contact pressure on the leakage for different applied gas pressures and a combination of HY54 and bronze.

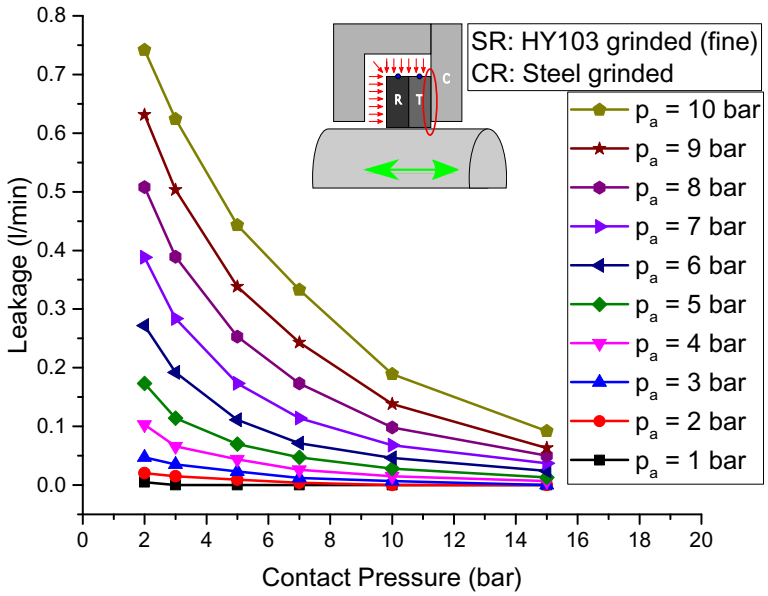

Figure 53: Influence of the contact pressure on the leakage for different applied gas pressures and a combination of HY103 and steel.

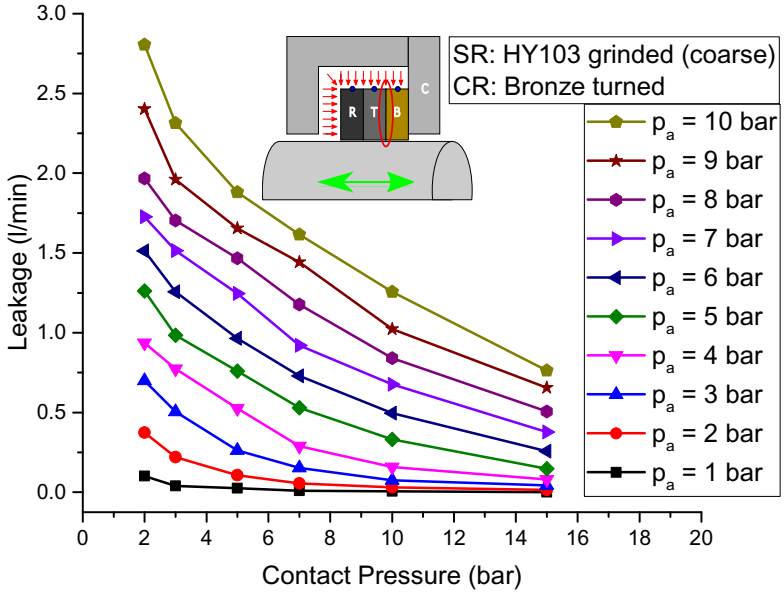

Figure 54: Influence of the contact pressure on the leakage for different applied gas pressures and a combination of HY103 and bronze.

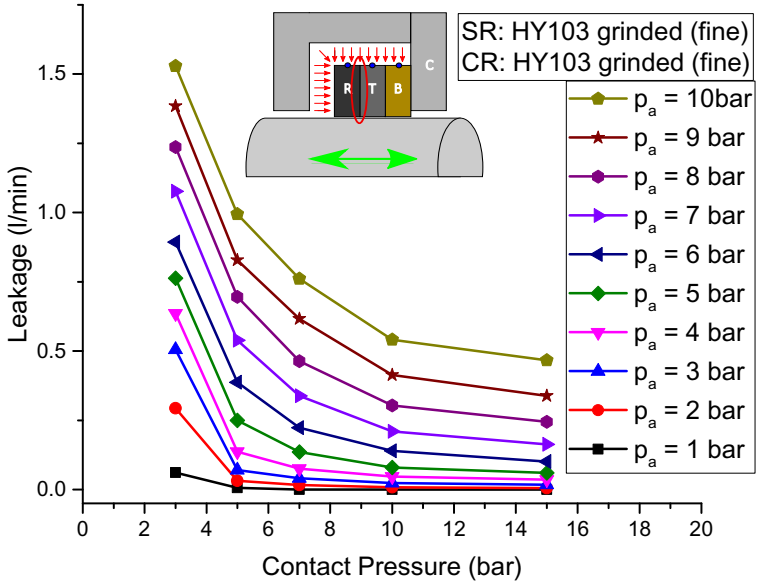

Figure 55: Influence of the contact pressure on the leakage for different applied gas pressures and a combination of HY103 and HY103.

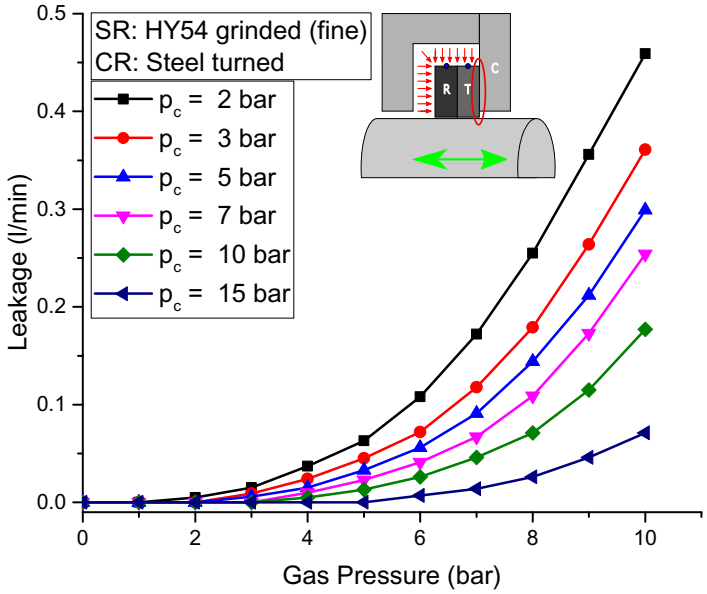

Figure 56: Influence of the gas pressure on the leakage for different contact pressures and a combination of HY54 and steel.

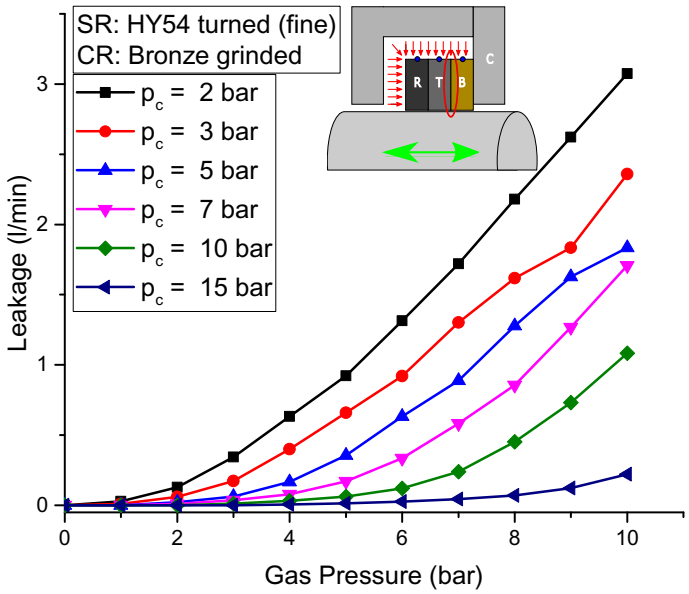

Figure 57: Influence of the gas pressure on the leakage for different contact pressures and a combination of HY54 and bronze.

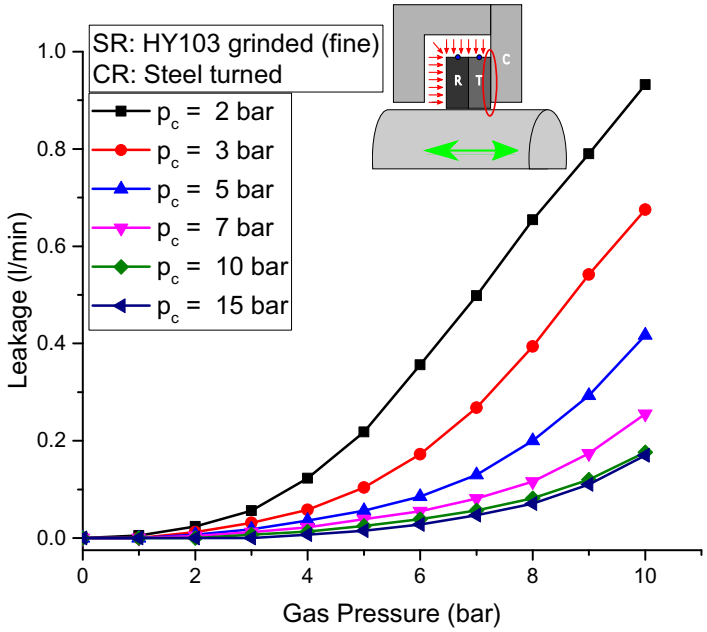

Figure 58: Influence of the gas pressure on the leakage for different contact pressures and a combination of HY103 and steel.

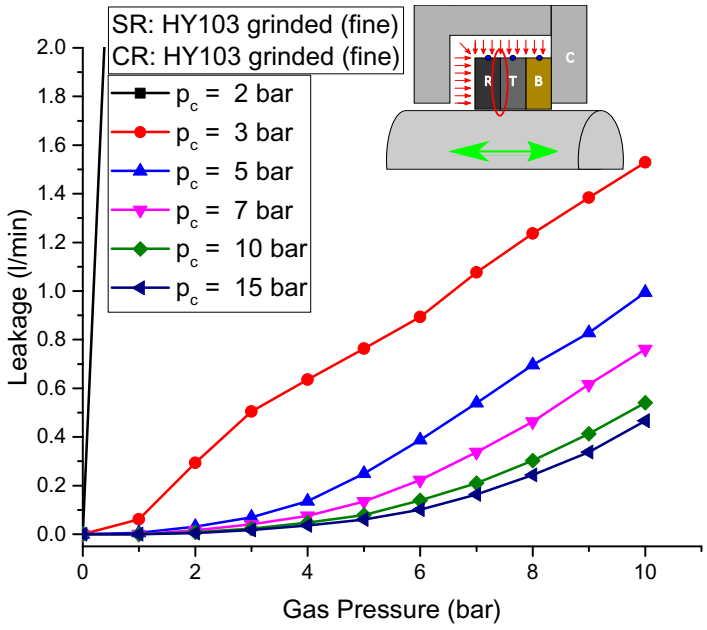

Figure 59: Influence of the gas pressure on the leakage for different contact pressures and a combination of HY103 and HY103.

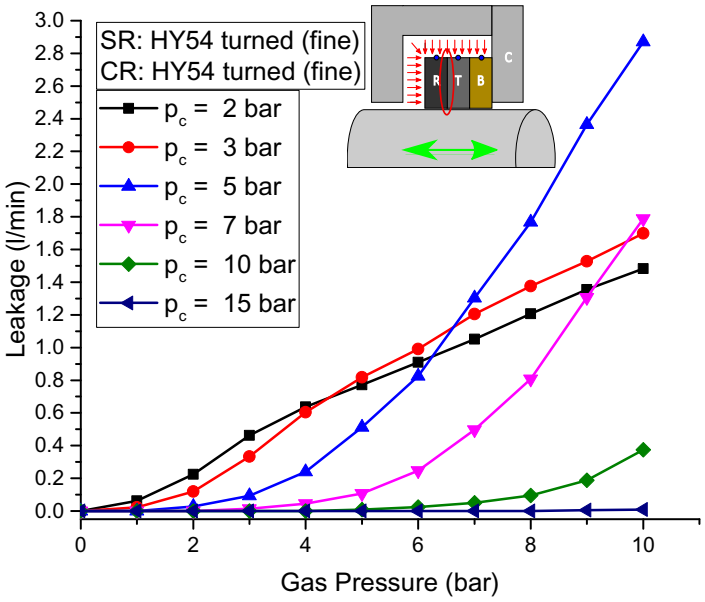

Figure 60: Influence of the gas pressure on the leakage for different contact pressures and a combination of HY54 and HY54.

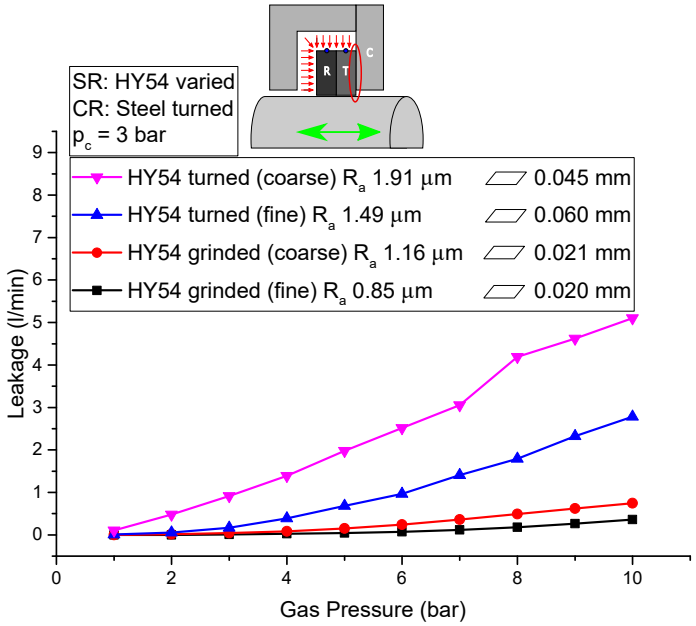

Figure 61: Influence of the manufacturing method of HY54 rings on the leakage for a contact and gas pressure of 3 bar and a combination with steel.

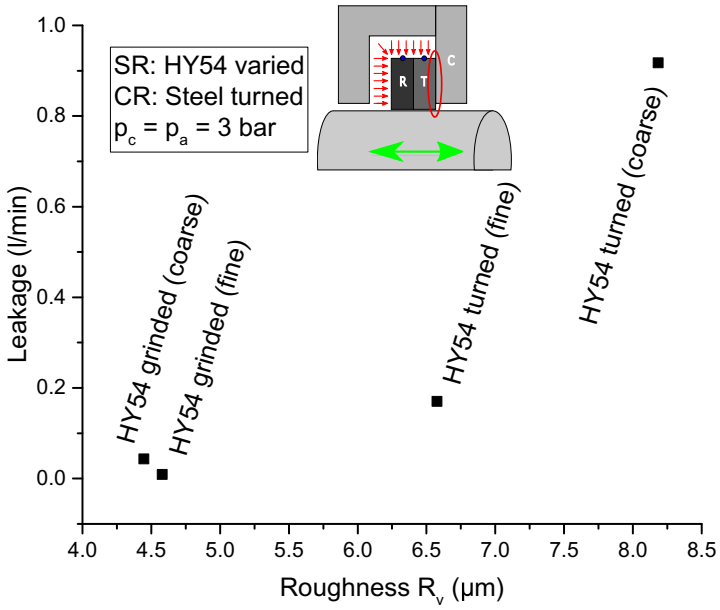

Figure 62: Influence of the roughness R_v of HY54 rings on the leakage for a contact and gas pressure of 3 bar and a combination with steel.

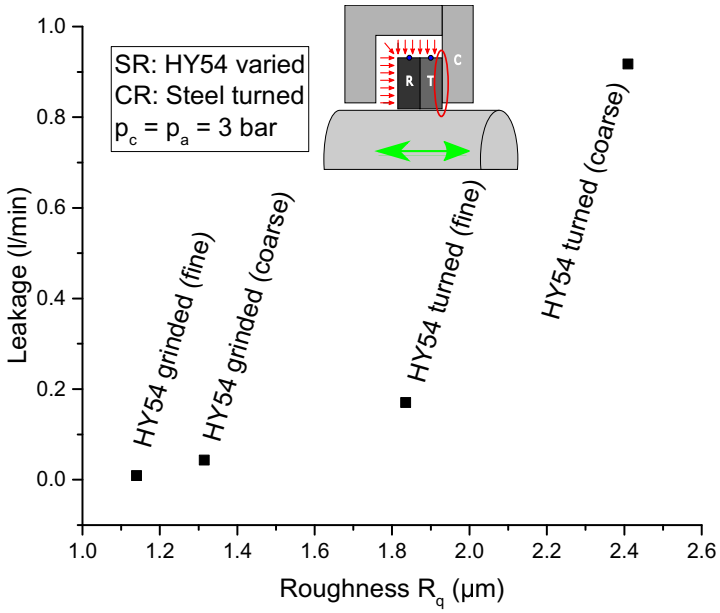

Figure 63: Influence of the roughness R_q of HY54 rings on the leakage for a contact and gas pressure of 3 bar and a combination with steel.

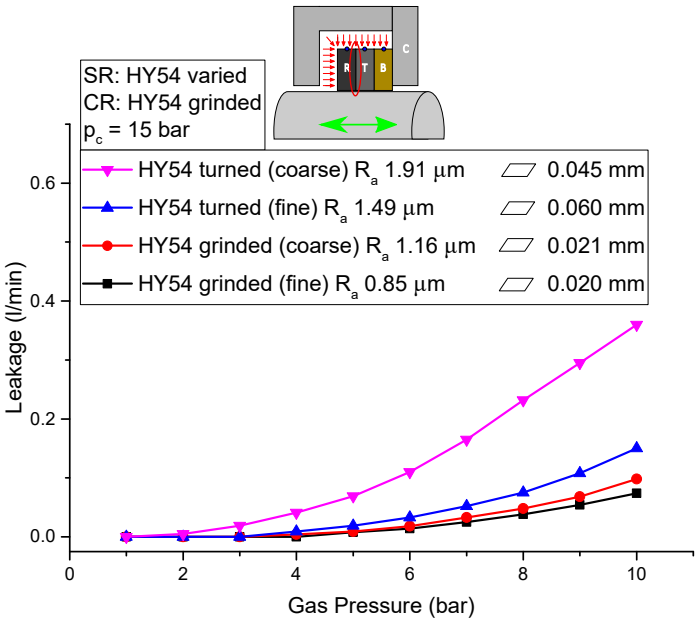

Figure 64: Influence of the manufacturing method of HY54 rings on the leakage for a contact pressure of 15 bar and a combination with HY54.

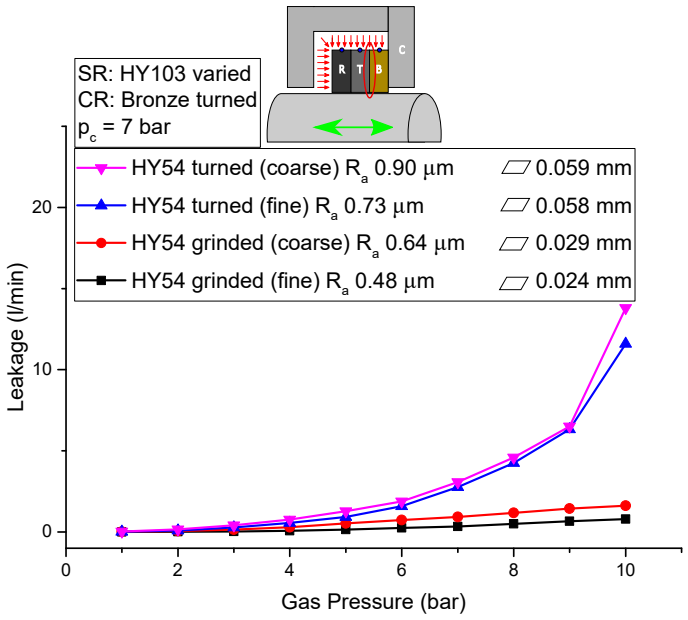

Figure 65: Influence of the manufacturing method of HY103 rings on the leakage for a contact pressure of 7 bar and a combination with bronze.

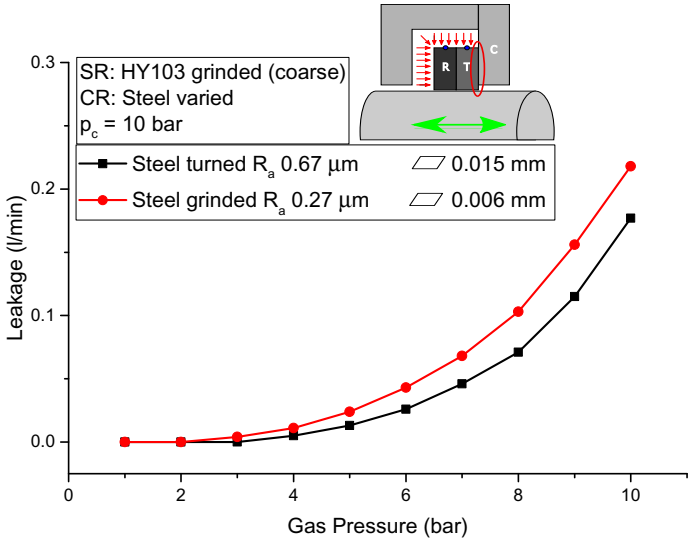

Figure 66: Influence of the manufacturing method of the steel ring on the leakage for a contact pressure of 10 bar and a combination with HY103.